# RELIABILITY ASSESSMENT OF A REINFORCED CONCRETE CHIMNEY UNDER SEISMIC AND WIND LOADING BY USING STRUCTURAL HEALTH MONITORING

by

Mehmet Orçun Tokuç

B.S., Civil Engineering Department, Yıldız Technical University, 2003,

M.S., Earthquake Engineering, İstanbul Technical University, 2008

Submitted to the Institute for Graduate Studies in
Science and Engineering in partial fulfillment of
the requirements for the degree of
Doctor of Philosophy

Graduate Program in Civil Engineering

Boğaziçi University

2015

*DEDICATION*

*To*

*my precious love, Bahar*

*and*

*my beautiful daughter, Zeynep*

# ACKNOWLEDGEMENTS

I would like to express my sincere gratitude and appreciation to Assoc. Prof. Serdar Soyöz for his invaluable guidance and help during the preparation of this dissertation.

I would like to thank for his leading me into the field of structural health monitoring and valuable guidance to my experience in engineering practice, his patience and encouragement during the preparation of this thesis.

I would like to thank Assoc. Prof. Hilmi Luş and Asst. Prof. Ufuk Yazgan for their kind support and valuable advices to make always a better work.

I would like to thank Prof. S.Semih Tezcan, whose work and insights give me an inspiration and the depth to solve engineering problems.

I am also thankful to Tamer Tunca and Naci Endem for their support and leading me into the field construction of the chimney. Tamer Tunca introduced me every details about the design and construction of a chimney, chimney society etc. and I would like also to thank for his patience and cooperation during my thesis period.

In addition, I would like to express my deepest gratitude to my parents for their infinite encouragement during all my life. Unfortunately, I lost my father toward the end of thesis duration, Halit Tokuç, who will be proud of me completing this work if he is alive. His memory will always be with me.

Last but not the least, I am very thankful to my wife, Bahar, without her, this thesis would not have been possible. Her incredible tolerance was indescribable. I must mention one more person, my daughter, Zeynep. She was born in the middle of this study and she was my main motivation during this study.

# ABSTRACT

## RELIABILITY ASSESSMENT OF A REINFORCED CONCRETE CHIMNEY UNDER SEISMIC AND WIND LOADING BY USING STRUCTURAL HEALTH MONITORING

This study presents the reliability assessment of a 100.5 m tall reinforced concrete chimney at a glass factory under earthquake and wind loading by using structural health monitoring (SHM) tools. Ambient vibration measurements were taken and recorded in order to identify modal parameters of the chimney. Modal frequencies and shapes were vibration-based identified by using Frequency Domain Decomposition (FDD) method. In addition, damping ratio of the chimney was identified by carrying out random decrement signature technique (RDST). FEM of the chimney was built up based on design drawings and then updated by using identified modal parameters. Updated and non-updated models were considered for reliability assessment of the chimney under wind and earthquake loadings. As for earthquake loading, probabilistic seismic hazard analysis (PSHA) was carried out to determine earthquake demand distribution of the chimney under an earthquake scenario. Demand distribution of the chimney was developed by performing linear time history analyses under selected earthquake records resulting from PSHA results. On the other hand, multivariate stochastic wind fields were generated along the height of chimney. Demand distribution of the chimney was developed under repetitive seeds. Capacity distribution of the chimney's base section was also developed by using Monte Carlo simulation for both earthquake and wind loading. Eventually, capacity and demand distribution of the system were obtained both for updated and non-updated cases under two types of loading. The reliability estimation was performed for non-updated FEM with 5% damping ratio and updated model with identified damping ratio by using RDST.

# ÖZET

## BETONARME BİR BACANIN YAPI SAĞLIĞI İZLEMESİ KULLANILARAK DEPREM VE RÜZGAR YÜKLERİ ALTINDA GÜVENİLİRLİĞİNİN DEĞERLENDİRİLMESİ

Bu çalışma, bir cam fabrikasında yer alan 100.5 m yüksekliğinde betonarme bir bacanın yapısal sağlık izleme SHM araçlarını kullanarak deprem ve rüzgar yükleri altında güvenilirlik değerlendirmesi sunar. Ortam titreşim ölçümleri baca modal parametreleri belirlemek için alınmış bve kaydedilmiştir. Modal frekansları ve şekilleri titreşim esaslı frekans dağılımı FDD yöntemini kullanarak tespit edildi. Buna ek olarak, baca şönümleme oranı rastgele azaltma imza tekniği RDST yaparak tespit edilmiştir. Bacanın sonlu eleman modeli tasarım çizimleri göz önünde bulurak yapılmış ve tespit edilen modal parametreler kullanılarak güncellenmiştir. Güncel ve güncel olmayan modeller rüzgar ve deprem yükleri altında baca güvenirlik değerlendirmeşi için elde edilmiştir. Deprem yüklerine gelince, olasılıksal sismik tehlike analizi PSHA bir deprem senaryosu altında bacanın deprem talep dağılımını belirlemek amacıyla yapılmıştır. Baca Talep dağılımı PSHA sonuçları ile seçilen deprem kayıtları alında zaman tanım aralığında çözüm lineer analizleri yapı elde edilmiştir. Öte yandan, çok değikenli stokastik rüzgar alanları baca yüksekliği boyunca oluşturulmuştur. Baca talep dağılımı tekrarlayan hareketler altında geliştirilmiştir. Baca taban kesitinin kapasitesi dağılımıda hem deprem ve rüzgar yükleme için Monte Carlo simülasyonu kullanılarak geliştirilmiştir. Sonunda, sistemin kapasitesi ve talep dağıtımı her iki yükleme altında güncel ve güncel olmayan durumlar için elde edilmiştir. Güvenilirlik tahmını % 5 sönüm oranı güncellen meyen model ve RDST kullanarak oranı sürümleme oranı belirlenen güncellenen model için belirlendi. Sonuç olarak, yapısal parametreleri güncellenen sistemin güvenirliliginin, yapısal parametreleri güncellenmeyen sisteme kiyasla düşük olduğu gösterilmiştir.

# TABLE OF CONTENTS

# LIST OF FIGURES

# LIST OF TABLES

# LIST OF ACRONYMS/ABBREVIATIONS

| | |
|---|---|
| ACI | American Concrete Institute |
| CICIND | International Committee on Industrial Chimneys |
| COV | Coefficient of Variation |
| FEM | Finite Element Model |
| FDD | Frequency Domain Decomposition |
| FFT | Fast Fourier Transform |
| GMPE | Ground motion prediction equation |
| MAC | Modal Assurance Criteria |
| PSHA | Probabilistic Seismic Hazard Analysis |
| RDST | Random Decrement Signature Technique |
| UHS | Uniform Hazard Spectrum |

# 1. INTRODUCTION

Tall buildings and special structures have been always popular research base since for many decades not only in the field of earthquake engineering but also wind engineering. Industrial chimneys are one of the most important ones in this area and therefore a reinforced concrete chimney is selected as the subject of this study.

## 1.1. Generic View of the Chimney

A chimney is a structure which provides ventilation for hot flue gases or smoke from a boiler, furnace or incinerator to the outside atmosphere. Chimneys are typically vertical structures that gases flow smoothly and draw air into the combustion what is known as stack. The space inside a chimney is called flue.

A flue gas stack (industrial chimney) is a special type of chimney, a vertical pipe, channel or similar structure through which combustion product gases called flue gases are exhausted to the outside air. A chimney is typically composed of two parts.

- Concrete Shaft (Windshield)
- Liner (flue)

Liner (flue) is the part that flue gases are exhausted to the outside air. Concrete shaft serves as a shelter that protects the liner from external effects such as wind and

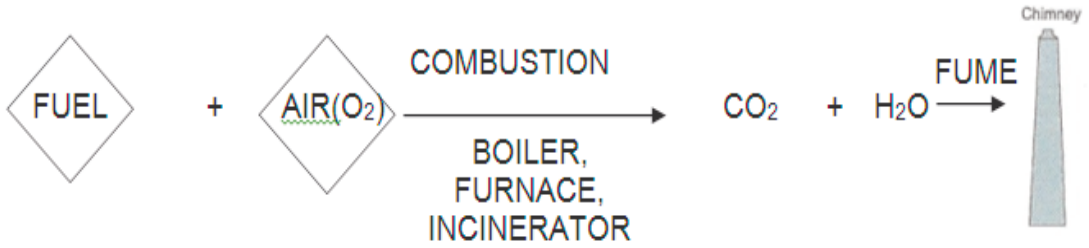


Figure 1.1. Process of Combustion Ending with Chimney.

earthquake. Concrete shaft is also known as windshield. Figure 1.2 presents the typical cross section of a chimney.

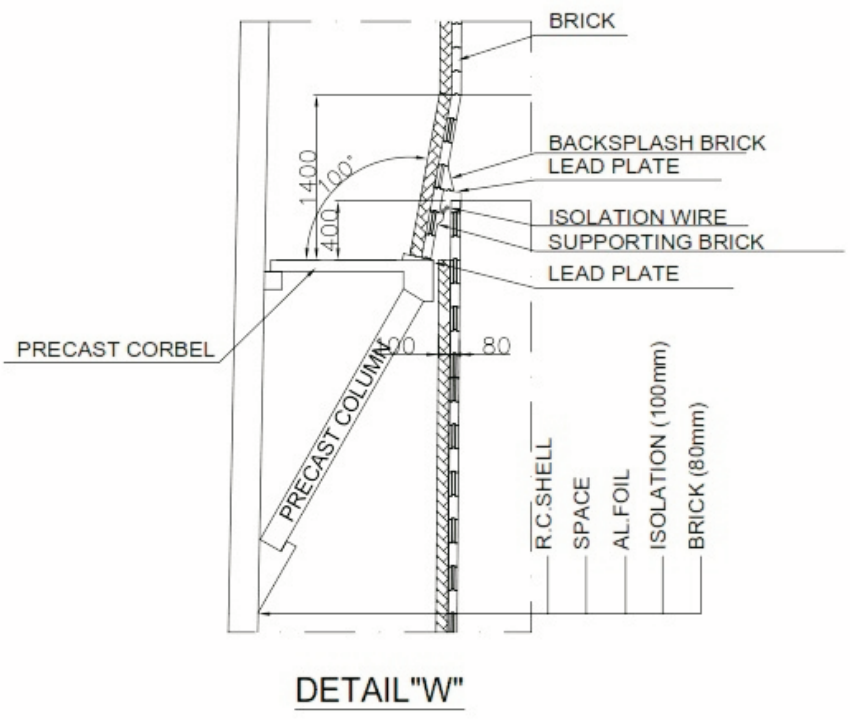


Figure 1.2. Typical Cross Section of the Chimney (ENDEM Co).

### 1.1.1. Types of Chimney

There are many types of chimney in terms of drafting type of gas, inlet temperature of the chimney, liner types. These are;

- Drafting Type of Gas
  - (i) Natural Draft (Gas Pressure @bottom<Atmospheric Pressure
  - (ii) Forced Draft (Gas Pressure @bottom>Atmospheric Pressure

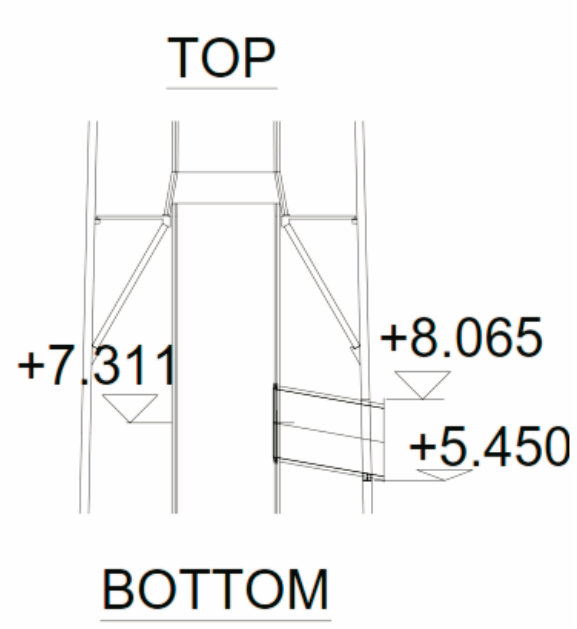


Figure 1.3. Flue Duct Entrance (ENDEM Co).

- Inlet Temperature of the Chimney
  - (i) Wet Chimneys (Gas Temperature $< 54\ ^oC$ )
  - (ii) Cold Chimneys (Gas Temperature $< 100\ ^oC$ )
  - (iii) Warm Chimneys ($100\ ^oC <$ Gas Temperature $<300\ ^oC$
  - (iv) Hot Chimneys (Gas Temperature $> 300\ ^oC$)

- Liner Material Type
  - (i) Brick Liner
  - (ii) Steel Liner

### 1.1.2. Calculation the Height of a Chimney

One of the most important geometric characteristic of a chimney is its height, because it affects the stiffness and magnitude of the loads. It certainly depends on journey of the gas along the chimney. A gas particle moves due to pressure difference. Drafting the gas from the atmosphere occurs due to the fact that the unit weights of

the gas and atmosphere are different. Natural draft (D) can be expressed as;

$$D = H_s(\gamma_{air} - \gamma_{gas}) \tag{1.1}$$

where; $\gamma_{air}$ Specific weight of air, is the $\gamma_{gas}$ Specific weight of gas in flue, $H_s$ is the distance between elevation of flue duct entrance and the top elevation where gas draws into air.

The service pressure at elevation entrance flue duct is determined depending on the capacity or the type of boiler.

During the journey of gas, gas bears some losses that are;

- Exit Losses

$$L_{ex} = \gamma_t \frac{v_t^2}{2g} \tag{1.2}$$

- Friction Losses

$$L_{fr} = 0.04. \frac{H_s}{D_m} \gamma_m \frac{v_m^2}{2g} \tag{1.3}$$

- Entrance Losses

$$L_{ent} = 1.5 \gamma_b \frac{v_b^2}{2g} \tag{1.4}$$

- Velocity Variation Losses

$$L_v = \gamma_m \frac{v_t^2}{2g}(1 - (\frac{v_b}{v_t})^2) \tag{1.5}$$

Net Draft can be calculated such as;

- Net Draft = -Natural Draft + Losses

### 1.1.3. Construction Method of the Chimney

The construction method of the chimney is important because it influences static and dynamic properties of the chimney. The behavior of stack-like structures is represented by a cantilever distributed system. There is no diaphragm use in conventional chimney construction unless otherwise requested by the owner. Mass and stiffness are distributed along the height; therefore continuous form should be maintained. In addition, as indicated above, liner of the chimney can be constructed using brick or steel material. Additional mass due to the geometry of liner is transmitted to the concrete shell of the chimney.

Liners may be constructed such that they increase the overall stiffness of the chimneys e.g. the ones in Russia and Czech Republic. This means that stiffness of the liner can not be transmitted to the shell concrete part of chimney. For this reason, liner is hanged on the platforms which are most commonly built as precast reinforced concrete slabs and columns or corbels (Figure 1.4).

Figure 1.4. Brick Liner Construction on Precast Slabs (ENDEM Co.).

These precast members are pin connected to the shell part of the chimney. (Figure 1.5). Thus, there is no contribution to the overall stiffness from the liner but the weight of the liner is transmitted to the shell.

Figure 1.5. Precast RC Members and their Connections (ENDEM Co.).

Slipforming operation is used to provide continuous form of the chimney. Most chimneys have a tapered geometry, therefore slip form is a very handy tool that adjust the diameter and thickness varying along the height of the chimney. Slipform must not be stopped at any elevation during the construction of shell due to the fact that cold joints con occur when slipforming stops. Figure 1.6 presents typical cross section of slipforming.

The slipform system which is used for the construction of this chimney shaft is widely known as the AHL system. The operation of this system is briefly explained below. Jacking rod A is located centrally in the concrete wall. Jack B slides upward on A, taking yoke C with it. The following are attached to C, inner and outer shuttering F, external and inner working platform D, scaffolding for adjustment H, and hanging scaffolding I. A draw tube E is suspended centrally under yoke C so that, on completion off the shaft, jacking rod A can be withdrawn and used again.

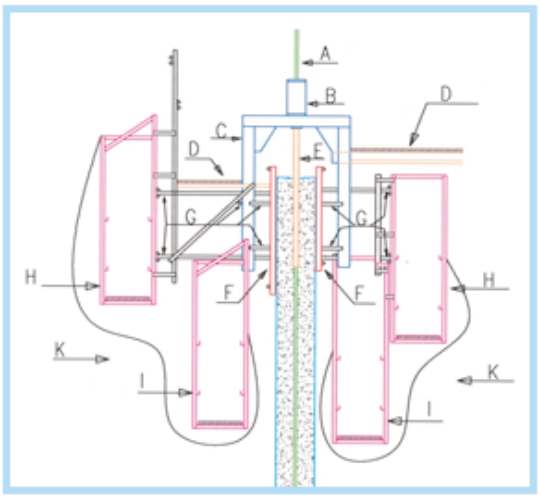


Figure 1.6. Typical Cross Section of Slipform (ENDEM Co.).

The hanging platform I permits trowelling of the concrete surfaces and application of curing compounds during sliding as well as the exposing of projecting reinforcement bars for corbels, dowels. Raising of the shuttering is affected by means of the double-acting jacks B which work in unison and feature a lifting capacity of 6 tons. Attachment and lifting of the 28 mm diameter jacking rod A are effected by a simple rugged and reliable gripper head mechanism. The sequence of work during slipforming necessitates

constant and thorough checking, which is carried out by optical plumbing devices, thus resulting in maximum dimensional accuracy. The diameter, wall thickness of the shaft is controlled by the spindels G at every 25 cm of rise.

Figure 1.7. Setup Slipforming (ENDEM Co.).

During the slipform concreting procedure, the rate of lifting of slipform is based on; concreting and setting rate of concrete. Rate of fixing rebar, block out and any adjustment may be necessary for alignment. Average of lifting and jacking rates i.e. 125 mm / hr (Figure 1.7).

Figure 1.8. Construction Phase of the Chimney (ENDEM Co.).

At the beginning of phase of concreting, the concrete the concrete is transported, by mobile crane or mobile pump, to the top part of desk from ground then deposited into the hoppers on the top part of deck and distributed to the chute by wheel barrows to the slipform shell. After 30 meters concrete is supplied by service hoist, until the

top of chimney. The service hoist shall be also used to transport workers and materials (Figure 1.8).

### 1.1.4. Dynamic Properties of a Distributed System

In the literature, stack-like structures are represented as a cantilever distributed system. The dynamic properties of a uniform distributed cantilever beam is well known. The natural vibration mode can be typically calculated as in Equation 1.6.

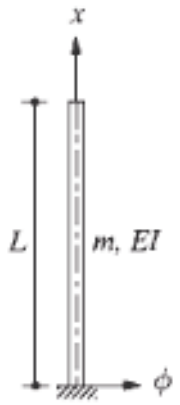


Figure 1.9. Uniform Cantilever Distributed System.

$$\phi_n(x) = C_1 \left[ \cosh \beta_n x - \cos \beta_n x - \frac{\cosh \beta_n L + \cosh \beta_n L}{\sinh \beta_n L + \cos \beta_n L} (\sinh \beta_n x + \sin \beta_n x) \right] \quad (1.6)$$

$$\beta_n{}^4 = \frac{\omega_n^2 m}{EI} \quad C_1 \quad (1.7)$$

$\beta_n L$ values for the first four modes of the system are obtained 1.8751, 4.6941, 7.8548 and 10.996, respectively. For n>4 this value can be computed as

$$\beta_n L \cong (2n-1)\pi/2 \quad (1.8)$$

Modal analysis of forced dynamic response equation is written

$$M_n\ddot{q}_n(t) + K_n q_n(t) = P_n(t) \tag{1.9}$$

The *generalized mass Mn and generalized stiffness Kn* can also be written as

$$M_n = \int_0^L m(x)[\varphi_n(x)]^2 dx \tag{1.10}$$

$$K_n = \int_0^L EI(x)\left[\varphi_n{}''(x)\right]^2 dx \tag{1.11}$$

and for the *nth* mode are related:

$$K_n = \omega_n^2 M_n \tag{1.12}$$

Generalized mass and stiffness matrixes are obtained for a 100 m tall chimney as follows:

$$K_n = \begin{bmatrix} 28816 & & & \\ & 819600 & & \\ & & 5.85.10^6 & \\ & & & 2.194.10^7 \end{bmatrix} kN/m \tag{1.13}$$

$$M_n = \begin{bmatrix} 1650.6 & & & \\ & 1802.3 & & \\ & & 1848.2 & \\ & & & 1860.3 \end{bmatrix} kNs^2/m \tag{1.14}$$

The four mode shapes can be obtained by using mass and stiffness matrix. Figure 1.10 represents the four mode shapes of the system.The vibration periods of the chimney

can be calculated for the four modes as $T_1$= 1.504 sec, $T_2$= 0.295 sec, $T_3$= 0.116 sec and $T_4$= 0.058 sec, respectively. In Section 4, the period values of the chimney are obtained by using finite element model.The results obtained from using uniform distributed cantilever beam concept are different than the results obtained from FEM. This stems from the fact that tapered section along the chimney height is taken into consideration.

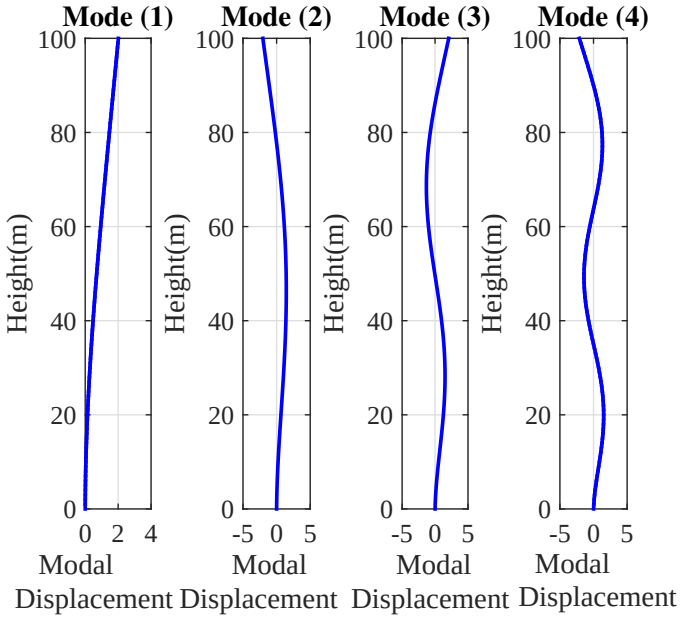


Figure 1.10. Four Mode Shapes of the System.

## 1.2. Literature Survey

Industrial facilities have great importance because the power demand of big cities such as New York, Istanbul, and Tokyo should be sustainable after a main disaster. If malfunction occurs in any part of these facilities, this causes considerable economical loss. This was experienced in Turkey after 1999 Kocaeli earthquake. Many buildings were collapsed and important structures such as hospitals, schools, refineries had remarkable damages. The demand of power is the primary need in order to sustain everyday life after a catastrophic event. Therefore, performance assessment of industrial facilities becomes important for earthquake prone regions.

After 1999 Kocaeli earthquake, a chimney constructed in Izmit Tupras Oil Re-

finery was collapsed. Many studies were carried out to investigate the reasons behind the failure.

Kilic and Sözen (2003) evaluated response of the collapsed chimney during Izmit earthquake. They built up finite element model (FEM) of the chimney by using constitutive material model. The chimney was analyzed under the strong ground motion data of Kocaeli earthquake. They found that collapse was more likely to occur around the large opening due to the fact that the first 20 seconds of the strong ground motion shaking represents an "impulse" loading in nature.

Huang *et al.*, (2004) assessed the performance of a collapsed chimney. Their investigation was focused on the dynamic response of the stack due to an earthquake motion recorded at a nearby site. In their paper the results of a response spectrum analysis of the Tupras stack and a generic U.S. stack were summarized. Then, a non-linear static analysis of the collapsed stack was presented using a demand-collapse comparison. The demand was represented by an acceleration-displacement response spectrum based on the recorded motion as well as some smoothed adaptations typical of design spectra, while the capacities were calculated from pushover curves using a non-linear reinforced concrete finite element analysis. They concluded that the carrying capacity around abnormally large rectangular opening at the stack did not meet earthquake demand.

Furthermore, performance-based assessment of a concrete chimney has been the subject of many researchers.

Goyal and Maiti (1997) examined inelastic seismic resistance of reinforced concrete stack-like structure. They presented a method that quantifies the inelastic seismic resistance of reinforced concrete stack-like structures by non-linear earthquake analysis.

The deformed configuration of stack was idealized as an assemblage of beam elements and actual stress and strain relationships of concrete and reinforcing steel were used to evaluate element matrices. Repeated non-linear analyses are performed by gradually increasing the intensity of acceleration time histories to a level where

collapse of the stack is observed in primary stresses. The set of time histories thus obtained are then used to define the ultimate intensity of ground motion that the stack can sustain if inelastic deformations are permitted. They also presented a procedure that quantifies the difference between inelastic seismic resistance and elastic seismic resistance in terms of displacement ductility capacity factors. For seismic design using available inelastic resistance, values of curvature ductility factor demand for the cross-sections of stacks were also presented. They concluded that whenever the ductile behavior of stacks is considered in design, the values of corresponding design shear force obtained from design basis earthquake spectrum needs to be enhanced.

An experimental research was also proposed by Wilson (2009). In his study, he documented an experimental study undertaken to investigate the cyclic behaviour of typical chimney sections with openings orientated to be bending critical and shear critical and the results were compared with previous tests with no openings. Significantly, no such cyclic tests have been previously been completed. The experimental results presented include; failure mode, over-strength factor, ultimate curvature, available ductility, hysteretic behaviour and strain distribution and the results were compared with some predictive analytical section models and design guidelines. He concluded that chimney sections with openings were not brittle, but were significantly less ductile than sections without openings.

Brownjohn *et al.*, (2010) instrumented a 183 m reinforced concrete chimney for a coal-fired power station in the latter part of its life during the construction of a replacement chimney. Because of concerns about large-amplitude response induced by interference effects from the new chimney in the prevailing upwind direction, a response monitoring system was installed, quickly followed by a tuned mass damper (TMD) system. As well as providing live display of the chimney response, the monitoring system was also used to check the functioning of the TMD. The monitoring system featured a direct implementation of the stochastic subspace identification procedure in the "virtual instrument" controlling the system, so that modal damping values for the system were displayed automatically, in real-time. The system thus provided an immediate visual indication of increased damping levels during strong winds, showing

the correct functioning of the TMD. The study describes the chimney, the monitoring system and its installation, the data processing and system identification procedure, together with performance data before, during and after installation of the TMD.

Wilson (2002) evaluated the inelastic response of tall reinforced concrete chimney structures bu using the results from an experimental program. The procedure is used to study the inelastic response of ten chimneys, ranging in height from 115 m to 301 m subject to earthquake excitation. Based on the study, a series of code design recommendations have been prepared and incorporated into the 2001 CICIND code to encourage reliance on the development of ductility in reinforced concrete chimneys and to prevent the formation of brittle failure modes. The basis for the selection of a structural response factor of R=2 which halves the seismic design forces is presented. The design recommendations result in both improved performance and cost savings of up to 20% compared with designs undertaken with the 1998 ACI307 and 1998 CICIND codes.

Gorski (2015) investigated the dynamic characteristics, i.e. the natural frequencies and structural damping ratios, of a tall industrial chimney, located in the power station of Belchatow in Poland, excited by the wind, based on GPS measurements using Random Decrement Method (RDM). The GPS receiver was able to measure only the first natural frequency of the chimney. The basic characteristics of a background noise of GPS technology based on the result of a static test were examined thoroughly. In order to increase the accuracy of GPS measurements as well as the dynamic characteristics estimation the filtering procedure using Type 1 Chebyshev band-pass digital filter was adopted. Then, the principles of RDM taking into account the influence of GPS measurement random noise were considered. The influence of filter parameters on the stability of the RD signature was also examined. Based on the filtered record of chimney dynamic response, the dynamic characteristics of the chimney were investigated using RDM for response considered in ten various directions in the horizontal plane. The results delivered some important practical information about two symmetry axes of the chimney. The effective investigation of a damping ratio should be made based on the analysis of the chimney response considered only in the directions of symmetry axes

of the chimney. The number of time segments of the chimney response taken into account in averaging of the RD signature as well as the time interval of the RD signature was also recommended. The obtained results proved that the dynamic characteristics of tall slender structures under wind excitations can be effectively determined based on GPS measurements using RDM.

Wind loading has long been an issue for owners of industrial facilities and engineers. Almost all industrial facilities such as refineries and glass factories have tall chimneys. Chimneys are one of the main parts of an industrial facility, if a malfunction occurs on the chimney, this creates significant economic loss. Furthermore, chimneys are affected by wind loading constantly during their service life. This highlights the priority of monitoring chimney performance under wind loading.

The studies that calculate the responses of structures under wind loading are generally based on. Davenport (1967) proposed gust factor approach in order to calculate the responses of structures under wind loading. The wind loading has mainly two parts that mean and fluctuation part. The gust part is formulized by a scale factor including the random effects of wind.

This approach may be not sufficient to ignore uncertainties in wind loading. Taking into consideration these uncertainties in wind loading, fluctuation part is generated stochastically. Simulation of random processes was developed and applied by several researchers in the literature.

Shinozuka and Jan (1972) made the first step regarding with generating multivariate stochastic process. They proposed a procedure that describes how to generate a digital simulation process as a series of cosine functions with weighted amplitudes, almost evenly spaced frequencies, and random phase angles.

Dynamic responses of tall buildings subject to stochastic wind loading were investigated by using different probabilistic methods (Zhang, 2008). They generated stochastic wind field along a tall building and applied wind loading on the structure by

using probability density evolution method (PDEM) and found that PDEM is applicable and efficient in the reliability analysis of wind-excited tall building. Uncertainties in structural properties may cause response of structure to deviate from actual response.

Vickery and Basu (1983) proposed a model for the prediction the response of chimneys to vortex shedding and the major characteristics of solutions employing the model were described. Simplified equations suitable for routine office use were derived. For modes other than fundamental the simplified forms require knowledge of the mode shapes and frequencies but, for the fundamental mode, it was shown that an equivalent static load can be defined with knowledge of the frequency only. The application of the simplified forms is demonstrated with sample calculations presented for two chimneys. The result of the simplified forms were shown to be slightly conservative in relation to estimates obtained using the detailed approach.

Menon and Rao (1997) reviewed the prevailing international codal procedures to evaluate the across-wind response of R/C chimneys. The disparities in the code based estimates of across-wind moments as well as the load factor specifications are examined from a reliability viewpoint. Conditions are also identified wherein the across-wind response, rather than the along-wind response, governs the design.

Cheng and Kareem (1992) proposed a study and in their study, the acrosswind response of isolated reinforced concrete chimneys of circular cross-section is studied using wind tunnel tests, full-scale measurements and response predictions based on semi-empirical methods. Three chimneys with available full-scale response observations were selected for this study to compare their measured and predicted responses. The wind tunnel experiments involved measurements of unsteady aerodynamic loads on rigid models of circular cross-section and aeroelastic response of scale models of full-scale chimneys. Tests were conducted initially on smooth surface models, which were repeated with artificially roughened surface. The acrosswind force spectrum measured on a rigid cylinder with the above surface roughness provides response estimates of chimneys with a good agreement with the observed full-scale response. With an appropriate selection of the aerodynamic parameters based on the far-field turbulence at

a site the predictive models provide more accurate estimates of the acrosswind response of concrete chimneys. The aeroelastic models of chimneys with the proposed roughness elements predict the acrosswind response of chimneys that have a good agreement with the observed full-scale response.

Vickery and Basu (1983) developed a mathematical model for two dimensional conditions. A key feature of model was the representation of the motion-induced force, which in reality involves complicated fluid-structure interaction phenomena. This representation was achieved through the inclusion of negative aerodynamic damping which was dependent on Reynolds number, on amplitude, and on the ratio of vibration frequency to shedding frequency. The principal characteristics of "lock in" condition were reproduced by using this approach.

In their second part of their study, Vickery and Basu implemented mathematical model to predict the across-wind response of tall slender structures of circular cross section to the wind.

This paper presents a semi-empirical mathematical model for predicting the across-wind response of tall slender structures of circular cross section to the wind. A computer program developed to obtain estimates of response for full-scale situations. The program was used compute the response of a 330 m TV tower and results were compared with the measured response. The buffeting forces which arise from lateral component of turbulence are identified. The difficulties associated with correctly scaling full-scale configurations in the wind tunnel make the measurement of many of parameters an uncertain source of data. The structural damping was the main uncertainty.

Vickery and Basu (1984) predicted vortex induced response of circular cross-section reinforced concrete structures and compared with observed full-scale behavior of seven RC structures of circular cross section. On average the predictions agree to within 5% with observations but had a large scatter attributable to model's failure to recognize the dependence of aerodynamic parameters on free stream turbulence.

The predictions showed a high level of scatter with a coefficient of variation of about 25%.Vortex shedding probably dominates the design about if the height to base diameter is less than about 13 or 14 for structures with no taper and less than about for strongly tapered structures, unless the above ratio is sufficiently small to raise the critical speed well beyond the design speed.

Considering the uncertainties in such systems, probabilistic assessment approaches are preferable than deterministic ones. Probabilistic assessment can be done statistically to find a reliability index of structure utilizing with basically load and resistance factor approach.

Load and resistance factor approach based on the fundamental principles of reliability have been investigated for decades (Shinozuka, 1983). This approach caused the development of a statistical framework for reliability-based design.

Furthermore, some studies have been conducted to determine resisting factor for probability-based design of the tubular reinforced concrete sections (Kareem, 1988). In this study, statistical analysis of the moment capacity of a tubular reinforced-concrete (R/C) section is performed. In this study, statistical the moment capacity of the cross section was estimated utilizing a second-order stress-strain relationship for concrete. The capacity of a cross section may vary due to variability in section properties, material strengths, and uncertainty associated with the prediction model. A systematic analysis of the propagation of uncertainties associated with these factors and their contribution to the overall uncertainty in the moment capacity was obtained based on the first-order second moment (FOSM) and Monte Carlo simulation techniques. A closed-form expression was derived for the uncertainty in the moment capacity following the FOSM approach. The FOSM approach provides results that were in good agreement with the Monte Carlo simulation. The results of a parametric study suggest that, for the example chimney, the coefficient of variation of the moment capacity was insensitive to the variation in the steel ratio. The analysis presented in this study would aid in determining resistance factors for probability-based design of the tubular reinforced-concrete members.

Few studies have been done to investigate the reliability of a reinforced concrete chimney under wind loading (Kareem and Hsiesh, 1986). They evaluated the risk of the chimney in terms of probability of failure. Both load effects and structural resistance were treated as random variables. They found that acrosswind response has a very significant influence on the probability failure of the chimneys.

## 1.3. Motivation of the Study

Even though performance-based concepts have good analytical and experimental base, the actual behavior of structures might be still different than estimated one due to many uncertainties. Structural health monitoring (SHM) tools allow us both to understand actual dynamic characteristics of structures and decrease uncertainties in modeling. Ambient vibration measurements can be taken remotely and automatically recorded and assessed. The dynamic parameters of structures such as frequencies, mode shapes, damping ratios can then be identified. Integration of SHM methods into performance assessment is, therefore, desired for detailed evaluation of existing conditions. Such evaluation can be even more beneficial for structures that are exposed to risks of high-intensity damaging events such as earthquake and wind loading. Considering the uncertainties in such systems, probabilistic assessment approaches are used in this study. Therefore, this study is intended to assess reliability of a 100.5m reinforced concrete chimney at a glass factory under earthquake and wind loading by using structural health monitoring. The existing conditions of the chimney are identified by using SHM methods and finite element model (FEM) of the chimney is updated to integrate the actual behavior. Reliability estimation of the chimney is obtained for non-updated and updated cases under earthquake and wind loading. The main contribution of this study can be expressed as follows:

- This study concerns with two main types of loading. These are earthquake and wind loading. Probabilistic seismic hazard analysis was carried out for earthquake loading and stochastic wind data were simulated for wind loading. Demand distribution considering uncertainties in these input motions and modeling assumptions was developed for a stack-like structure.

- SHM tools are utilized in order to identify current modal characteristics of the chimney. FEM updating procedures were applied to the chimney by using the results of experimental measurements. A reliability based framework was constructed to assess the chimney considering for both updated and non-updated cases under earthquake and wind loading.

## 1.4. Scope

This study is composed of eight chapters. The first chapter gives a general overview of the study and the literature survey.

Chapter 2 introduces chimney characteristics and the reasons why we should monitor the structures by means of SHM methods. In this chapter, the configuration of the mounted sensors on the chimney shell is presented. The reasons of selecting appropriate location of accelerometers are expressed.

Chapter 3 presents the system identification of the chimney. In the introduction of this chapter, a brief review of system identification is presented. Power spectrum density of vibration measurements is developed by using Frequency Domain Decomposition (FDD) method. The theoretical details of the FDD methodology are presented. Afterwards, modal parameters such as frequencies and mode shaped are obtained. In addition, the damping ratio are identified values by using random decrement signature technique (RDST). A mean damping ratio is calculated and compared with the values proposed in the literature.

Chapter 4 deals with finite element modeling (FEM) and updating. Initially, finite element model (FEM) of the chimney is presented. The details such as types of element, their numbers and boundary conditions used in the model are explained. In addition, the effect of uncertainties in modeling assumptions and structural properties on modal frequencies are shown. Afterwards, model updating procedure is briefly explained and MAC values calculated using correlation between mode shapes obtained in FE model and those obtained from identification are presented. Sensitivity analysis

is carried out to select appropriate updating parameters. Soil spring coefficient and Young's modulus are selected as updating parameters. Eventually, modal frequencies and mode shapes obtained for non-updated and updated FEM are plotted including identified results.

In Chapter 5, probabilistic seismic hazard analysis (PSHA) procedure for earthquake loading is described. Firstly, classical approach of PSHA is defined and then assumptions made in an improved model are presented. Afterwards, a plausible earthquake scenario is proposed and seismic hazard analysis is carried out in accordance with this scenario. Seismic hazard curves are developed and plotted. Deaggregation analysis results are obtained and seismic hazard maps are plotted for a given zone.

Chapter 6 deals with the wind loading and applications. Theoretical concepts are summarized regarding mean wind profile. Wind velocity fluctuation fields are simulated by using multivariate stochastic process. The basic concepts and formulas are expressed briefly. Verification of generated data is carried out by using random vibration concepts. The values of along-wind loading are obtained and subjected to chimney along the height. Power spectrum density of across-wind loading is plotted to indicate that it is not effective loading for this chimney.

Chapter 7 gives the reliability estimation results for both earthquake and wind loading. Firstly, demand distribution of the chimney is developed depending on overturning moment values at base of the chimney obtained under selected earthquake records utilizing PSHA results. Capacity distribution of the chimney section is also developed depending on ultimate moment capacity of chimney section at base by using Monte Carlo simulation.

As for wind loading, the procedure described above is the same. Demand distribution of the chimney was developed depending on overturning moment values at base of chimney obtained under many seeds utilizing multivariate stochastic process. Cracking moment capacity distribution of chimney section at base by using Monte Carlo simulation is developed.

Probability of failure values for each types of loading are obtained and comparison of results with specified literature is presented.

Chapter 8 presents some conclusions from this study and directions for future research.

# 2. CHIMNEY CHARACTERISTICS

The chimney is located in Bozuyuk, in the south east of the Marmara Region in Turkey and it is approximately 250-300 km far away from Istanbul. The chimney is 100.5 m tall and outer diameter is 9700 mm at base and 5750 at top. The wall thickness starts from 30 cm at the base and decreases to 20 cm at the top. It was constructed by ENDEM Construction Co. in 2012 .The concrete class used in construction is C 30 (fc'=30 MPa) Figure 2.1. presents the view of the chimney.

Figure 2.1. View of the Chimney at a Glass Factory Located in Bozuyuk.

Figure 2.2 presents the cross section of the chimney given in the design drawings. Figure 2.2 presents the elevation view of the chimney brick liner which is supported by precast slabs and columns at ten locations along the height of chimney. Circular foundation has a radius of 11.0 m and thickness of 2.5 m.

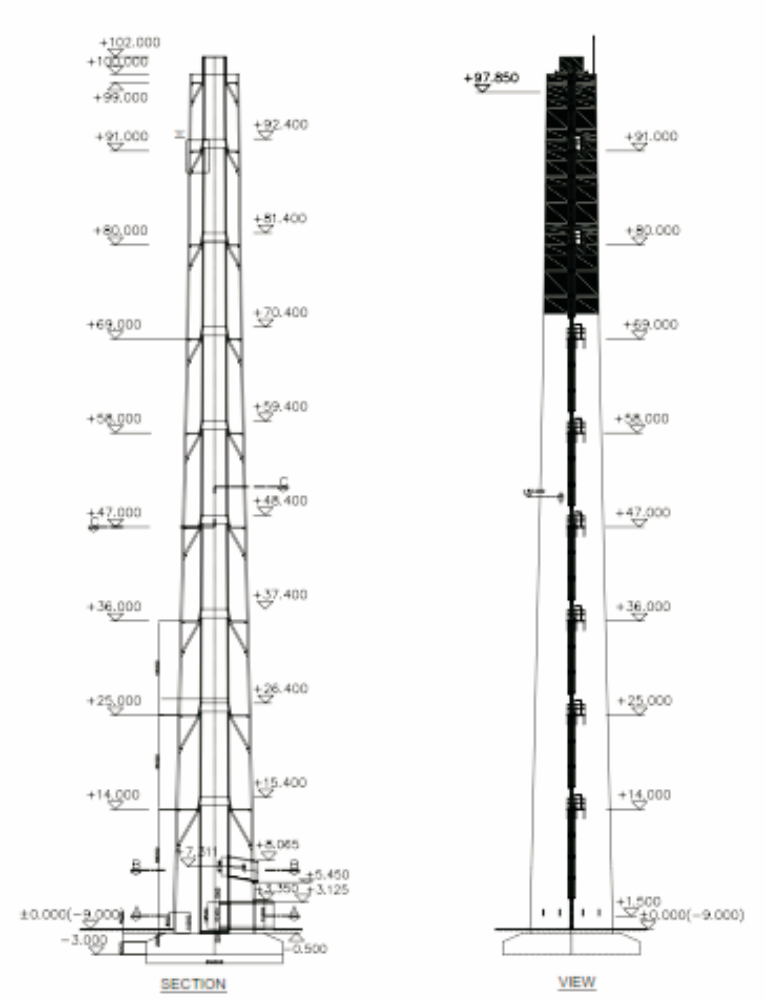


Figure 2.2. Elevation View of the Chimney.

Brick liner of the chimney is insulated to prevent shell of the chimney suffering damage due to high rise temperature.

Figure 2.3. Insulated Brick Liner.

The weight of brick liner is transmitted to shell part of the chimney by means of corbels. Precast slabs are pin connected to the shell part of the chimney.

Figure 2.4. Precast Slabs and Corbels.

The gas flow coming from heater first comes to flue duct then goes to brick liner. Refractory bricks are insulated with rock wool and corrugated steel to decrease temperature due to flue gas. Thus, the temperature between chimney shell and brick liner can be stayed constant (Figure 2.5).

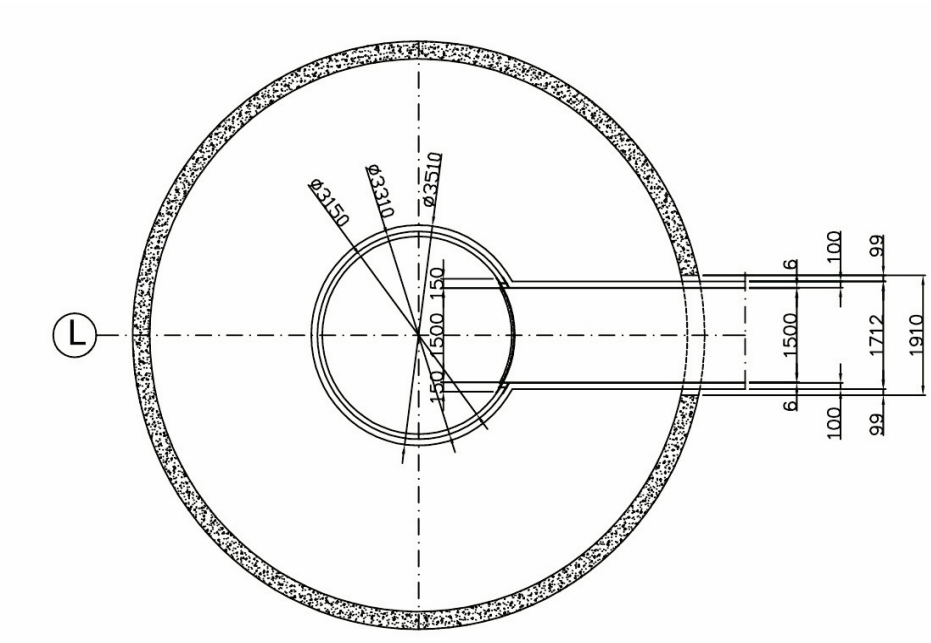


Figure 2.5. Layout of Base Section.

Openings around flue duct are vulnerable to effects caused by earthquake and wind loads. Therefore, additional reinforcement should be placed around the openings (Figure 2.6).

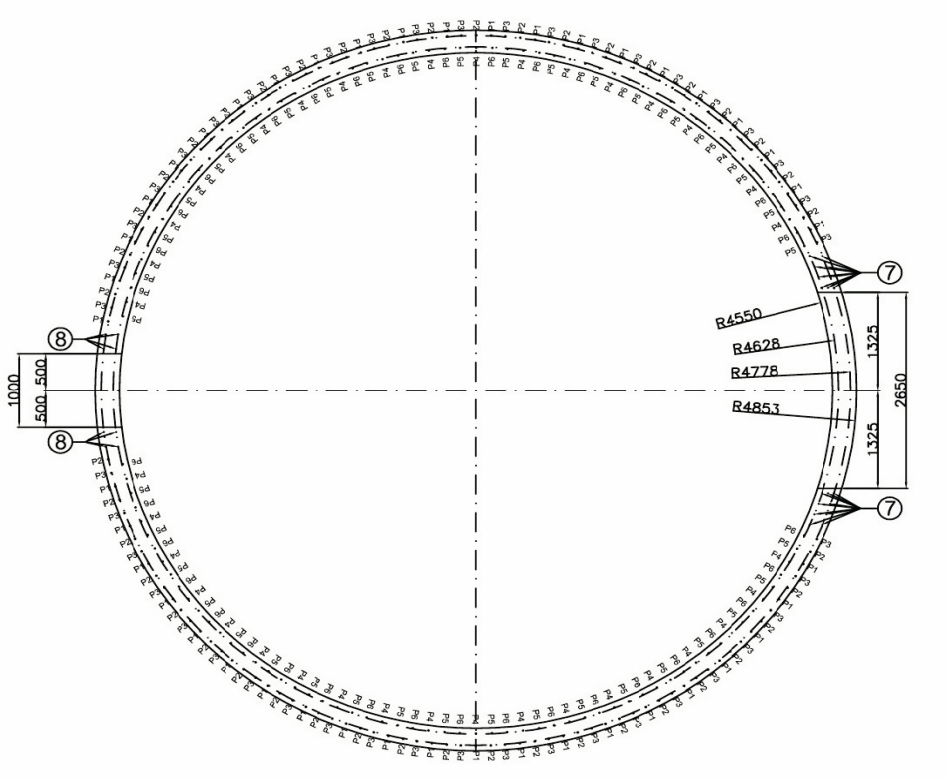


Figure 2.6. Section View of Horizontal Rebars.

# 3. SYSTEM IDENTIFICATION

## 3.1. Structural Health Monitoring

Structural Health Monitoring (SHM) is a process that provides accurate information regarding structural health condition and performance of engineering structures. The state of the structure must remain as specified in the design, although this can be influenced by normal aging due to usage, by the action of the environment, and by natural hazards such as earthquakes and storms which makes it possible to consider the full history database of the structure, and with the help of usage monitoring, it can also provide a prognosis (evolution of damage, residual life, etc.).

The reasons to monitor structures may be as follows:

- To determine the in-situ dynamic characteristics of the structure
- To check the design and analysis methods used.
- To develop new retrofit and strenghtening techniques
- To predict behavior for future extreme loads
- To detect and locate damage after an extreme event.
- To develop instantenous damage distribution.

SHM process involves selecting the excitation methods, the sensor types, number and locations, and the data acquisition/ storage/transmittal hardware. Economic considerations will play a major role in making these decisions. The interval at which the data should be collected is another consideration that must be addressed.

System identification is a method used to obtain the modal characteristics of an existing structure. Finite element based computer models is efficient tools that provide designer to understand the actual behavior of the structure under any impact such as wind, earthquake, explosion etc. Therefore, they have great interest for a design engineer and importance to be able to check the model. Furthermore, an existing structure

which is influenced by harsh environmental condition or has some deterioration due to aging should be monitored. Thus, this leads to developing of Structural Health Monitoring (SHM) systems. For these reasons, engineers try to find better solution to identify mechanical properties of an existing structure. There are two main types of system identification, input-output method and output-only method.

## 3.2. Input-Output Method

The input-output method is based on applying periodic force (input) on the structure, and measuring the response (output). Modal parameters are estimated by developing frequency response functions due to the periodic force. The structure is excited by moving the exciting device that attaches the structure. Thus, peak amplitudes at its own natural frequencies give the identified modal parameters. The frequency of the periodic input force is altered, and the exciting device is moved around the structure in several steps so that the structure is excited over a range of periods and spatial coordinates. Due to resonance behavior the structure will give higher amplitude at its own natural frequencies, which is the basis on which this method is established. This method requires some kind of structural excitation which can be of many different sorts. In small structures the excitation can be done with an impulse hammer, but for large structures the use of a large shaking device is necessary. These shaking devices can be quite expensive and inconveniently bulky.

## 3.3. Output-Only Method

The main advantage of this method is to use ambient vibrations, such as wind, traffic and minor tremors, to excite the structure. This means that no shaking device or impulse hammer is required to an initial motion; the method is simply based on using motion that is already there. This method is also called Operational Modal Analysis (OMA) because the analysis can be done while the structure is in operation. Since the input forces of the structure are not measured, special care must be taken to separate harmonic components of the loading from structural modes. Harmonic components are mostly relevant in mechanical engineering, where rotating machinery is the most

common source, but harmonic vibration can also be found in structures. Harmonic components which lie close to a structural mode may be mistaken for a mode, and should therefore be considered in the modal identification process.

### 3.4. Experimental Setup

Twelve accelerometers were mounted on the chimney shell to measure the vibration response. The chimney has eight access elevations for the refractory brick liner along the height of chimney. Appropriate location of accelerometers was selected to obtain largest modal displacements. Sensors were located at foundation level, +25.00, +58.00, +91.00, respectively. Main recorder was located at elevation +25.00. Figure 3.1 shows accelerometers located on chimney shell and the recorder.

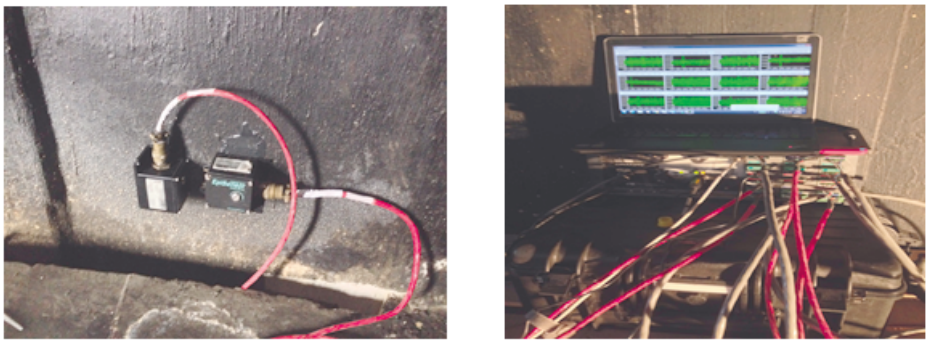

Figure 3.1. Accelerometers and the Main Data Recorder.

For each elevation, accelerometers were located both along x and y directions. Five accelerometers were mounted at the foundation level. Three of them were mounted vertically and used to monitor rocking mode. An additional sensor was located at elevation +91 m along x direction to monitor torsional mode of the chimney. Data acquisition system was monitored by using remote control via internet. Figure 3.2 shows the sensors location along the height of the chimney.

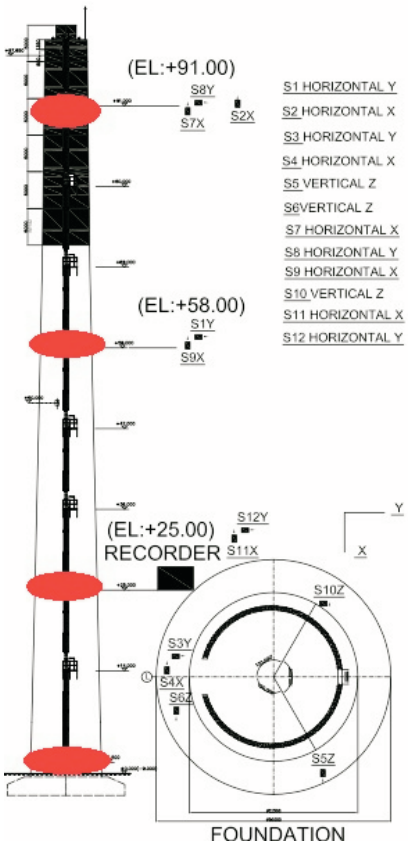


Figure 3.2. Sensor Layout along the Chimney Height.

In this study, ambient vibration measurements were recorded to identify modal parameters such as frequencies, shapes and damping ratios. Figure 3.3 presents a sample ambient vibration data recorded at elevation +25.00 and +91.00, respectively. Frequency Domain Decomposition (FDD) method (Otte *et al.*, 1990, Brinker *et al.*, 2001) was used to identify modal parameters.

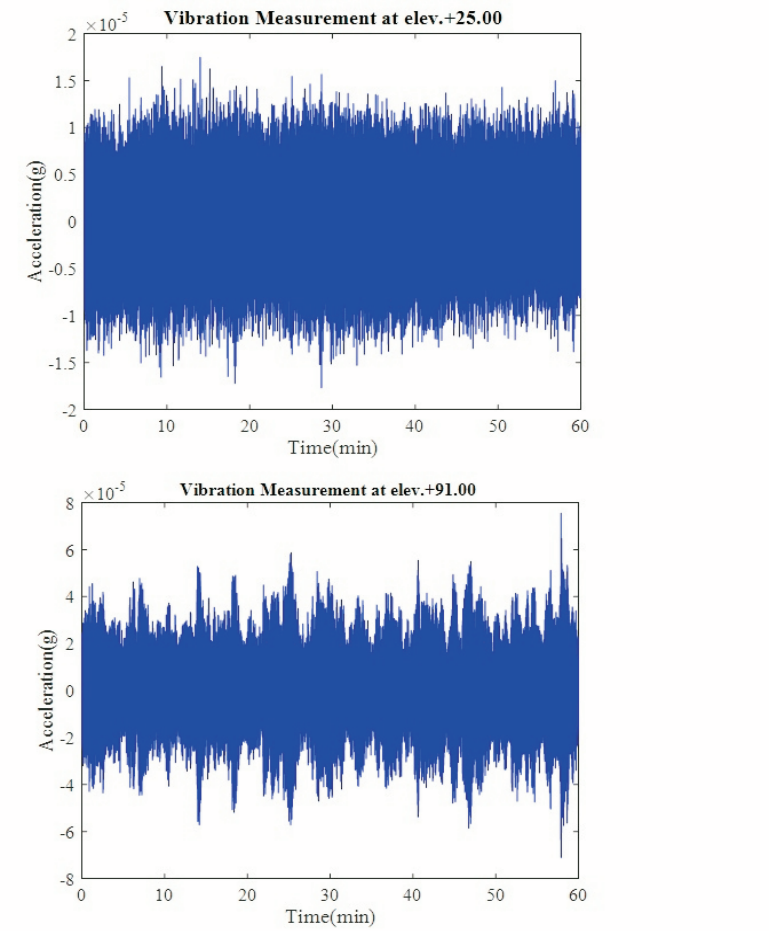


Figure 3.3. Ambient Vibration Measurements at Elevation +25.00 and +91.00.

In FDD method, first, cross spectral density matrix $S_{YY}(\omega)$ is generated from vibration data $Y(t)$ and is decomposed by singular value decomposition, (Equation 3.1),

$$S_{YY}(\omega) = U(\omega) \sum (\omega) U^H(\omega) \tag{3.1}$$

where, is the $\sum(\omega)$ diagonal matrix of singular values, is the $U(\omega)$ Unitary matrix of the singular vectors, is the superscript $H$ denotes the complex conjugate and transpose.

Power spectral density function was obtained plotting singular values obtained for each frequency values and the peak values were assigned as identified frequencies

of the chimney. Mode shapes of the chimney were the singular vectors.

$$\phi = U_{i1}(\omega) \tag{3.2}$$

and the corresponding singular value is the auto-PSD function of the corresponding SDOF system.This PSD function is identified around the peak by comparing the mode shape estimate with the singular vectors for the frequency lines around the peak. As long as a singular vector is found that has a high modal assurance criterion (MAC) value with , the corresponding singular value belongs to the SDOF density function.From the piece of the SDOF density function obtained around the peak of the PSD, the natural frequency and the damping can be obtained (Brinker *et al.*, 2001)

Figure 3.4 presents power spectral density of various responses recorded during a single day. From the figure, it is observed that the frequencies of the first, second, third modes are 0.59, 2.54, 6.01 Hz, respectively. The possible reason that a peak occurs around 3.9 Hz is mainly related to the fact that crude/vacuum heater unit in the main facility located very near the chimney that generates vibration when system is on.

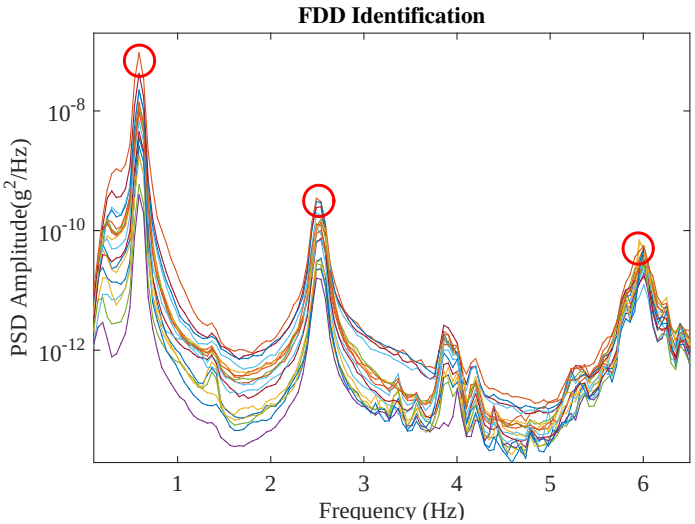


Figure 3.4. Spectral Densities for Selected Measurements.

## 3.5. Identifying Damping Ratio

Many techniques were developed in recent years, in order to obtain the dynamic properties of the structures from ambient vibration responses. They are based on the operational modal analysis and output only system identification. Random decrement signature technique (RDST) is one of them which allow damping analysis of the ambient vibration.

### 3.5.1. RD Signature Algorithm

Random decrement signature technique (RDST) is one of the tools to identify damping ratio of structures by using ambient vibration data. The concept of the technique was first presented by Cole (1979). He estimated the damping of a spacecraft by using this technique. In accordance with the concept, sub-segments are extracted from ambient vibration response selecting an appropriate initial condition called as triggering level. All sub-segments are averaged and a free decay function is obtained. The triggering level mostly is chosen as $\sqrt{2}\sigma$ or $\sigma$ which is standard deviation of random response. In this study, triggering level is selected as $\sqrt{2}\sigma$ RD signature concept can be expressed with Equation 3.3

$$z(\tau) = \frac{1}{N}\sum_{k=1}^{N} y(t_k + \tau) \tag{3.3}$$

where $z(\tau)$ is the RD signature, t is the time reference of the sub-segments, N is the number of averages, y is the recoded data, and is the time at which the triggering level is crossed.

### 3.5.2. Damping Estimation of the Chimney

Random responses of the chimney were recorded continuously for twenty four hours. RD signatures of each data set at the top of the chimney were developed. One of the representative RD signatures for the first and second mode is illustrated in Figure 3.5.

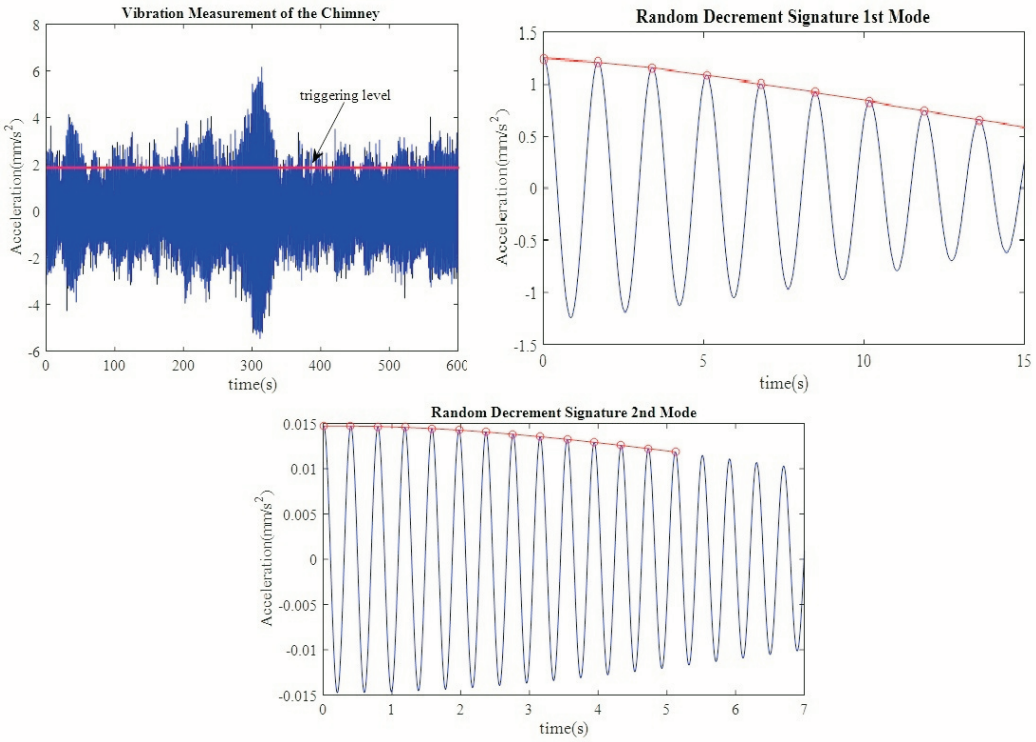


Figure 3.5. Vibration Measurement of the chimney and Random Decrement Signature for the First and Second Mode.

The damping ratio was calculated by using Equation 3.4 (Chopra, 2011).

$$\xi = \frac{1}{2\pi j} \ln \sqrt{\frac{u_i}{u_{i+j}}} \tag{3.4}$$

Amplitude dependent damping ratios were found for all recorded signals at the top of the chimney for the first and second mode. The signal processing tools are utilized to develop RD signature for the second mode. The signal is extracted containing frequencies 2.50 Hz and 2.60 Hz, which are the closest frequency values for the second mode, from the long data set. That is to say, band pass filter is applied within relevant frequency range in order to get the free decay function for the second mode. The damping ratio scattering with respect to amplitude is shown in Figure 3.6.

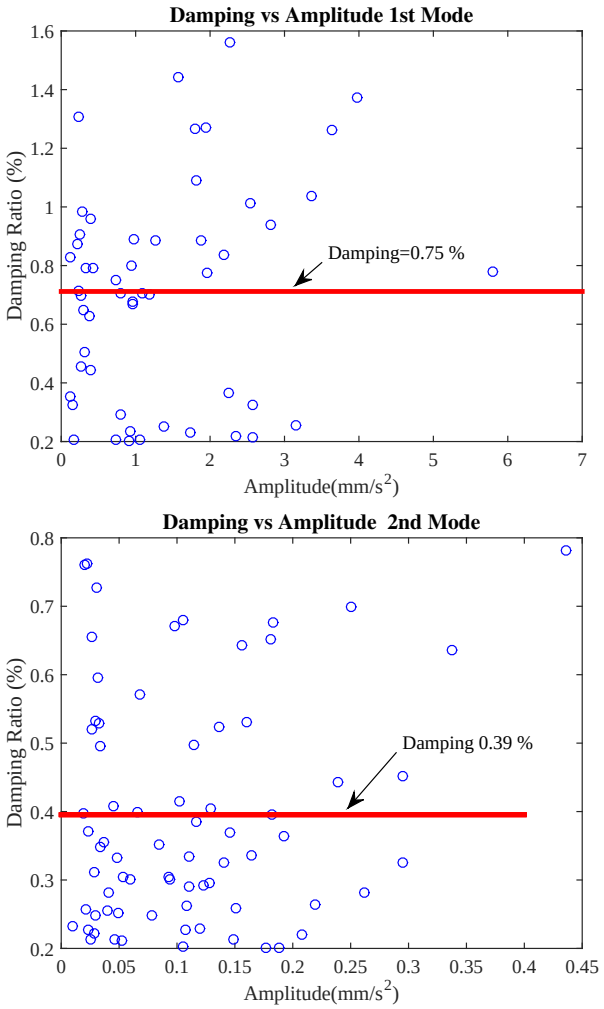


Figure 3.6. Amplitude-Dependent Values of the Chimney for the First and Second Mode.

The damping ratio value was identified as 0.75 % which is the mean value of the calculated damping ratios for the first mode and 0.39 % for the second mode. These values are used as the damping value for reliability assessment of the chimney for the updated FEM.

Table 3.1 presents the estimated damping values for a lined reinforced concrete chimney with foundation on gravel in the literature (Lupi and Niemann, 2013, Görski, 2015). It can be seen that the identified damping ratio for the first mode is in good agreement with the ones in literature.

Table 3.1. Damping Ratio Estimations.

| **Damping Ratios (%) (Concrete, Lined, Foundation on Gravel)** | | | |
|---|---|---|---|
| **Cicind** | **Eurocode** | **Lupi,Niemann** | **Gorski** |
| 1.51 | 1.11 | 0.73 | 0.56 |

# 4. FINITE ELEMENT MODELING (FEM) AND UPDATING

## 4.1. Finite Element Model of the Chimney

Finite element model (FEM) of the chimney based on design drawings was built up by means of SAP 2000. 18000 shell elements are used in the model including a foundation with soil springs. Refractory brick liner masses are assigned on the shell as additional mass. 6840 solid elements to model foundation and soil springs are assigned to the points of the mesh beneath foundation. Soil spring values were calculated by multiplying the subgrade modulus of soil with unit area.

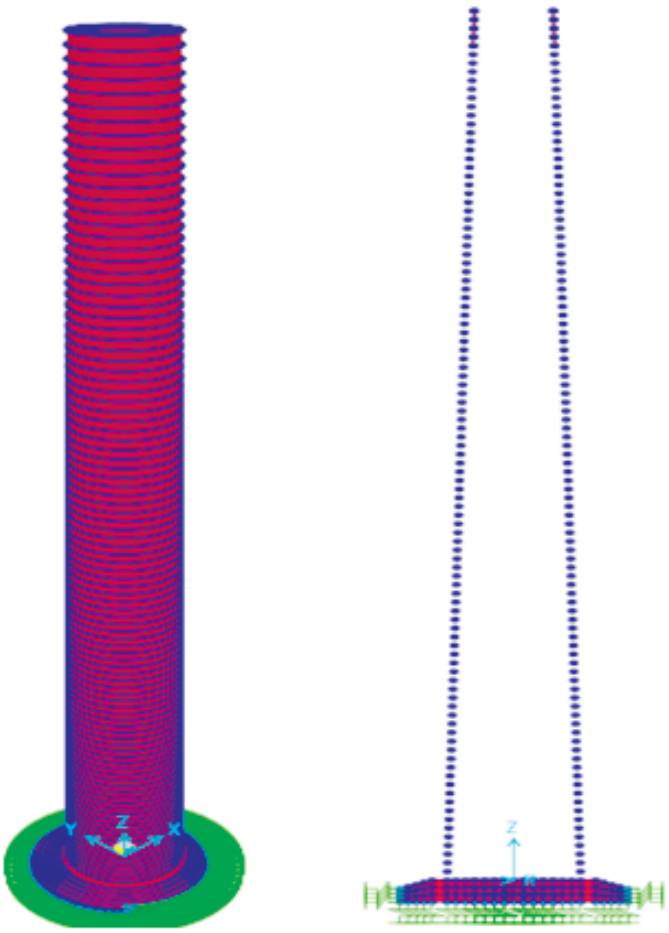

Figure 4.1. FEM of the Chimney.

Uncertainties in structural properties and modeling assumptions should be taken into consideration for FEM updating procedure. These uncertainties affect the reliability assessment process of the chimney.

### 4.2. Uncertainty in the Material (Structural) Properties

Young's modulus of concrete for specified concrete class is computed by different equations in accordance with codes.
TS 500 gives,

$$E_c = 3250\sqrt{f_c} + 14000(\text{MPa}) \tag{4.1}$$

ACI 318 gives,

$$E_c = 4700\sqrt{f_c}(\text{MPa}) \tag{4.2}$$

Eurocode (EN 1994) gives,

$$E_c = 22\left[\frac{(f_c + 8)}{10}\right]^{0.3}(\text{GPa}) \tag{4.3}$$

Finite element models (FEM) were built up for different Young's modulus values and analyzed.

Table 4.1. $1^{st}$&$2^{nd}$ Period Values Obtained for Different Young's Modulus.

| $1^{st}$&$2^{nd}$ Periods | | |
|---|---|---|
| PERIOD (sec) | | |
| TS500 | ACI 318 | EC1994 |
| E =31800 | E =25743 | E =32840 |
| 1.246 | 1.385 | 1.226 |
| 0.278 | 0.309 | 0.274 |

Table 4.1 indicates that the period of the chimney has different values for the equation of each Young's modulus given in the codes.

Generally, there is an opening near the base of the chimney for the liner (flue duct) that is the part of the chimney which gases are exhausted to the outside air. The effect of openings on first and second period of the chimney was investigated and values were tabulated in Table 4.2.

Table 4.2. $1^{st}$&$2^{nd}$ Period Values Obtained for the Model $w/$ and $w/o$ Openings.

| $1^{st}$&$2^{nd}$ Periods $(w/o)$ openings | $1^{st}$&$2^{nd}$ Periods $(w/)$ openings |
|---|---|
| TS500 | TS500 |
| E =31800 | E =31800 |
| 1.246 | 1.282 |
| 0.278 | 0.285 |

The difference was found as 3% in percentage between two cases. In accordance with results obtained from analyses above, uncertainties in material properties affect the fundamental period of the structure.

### 4.3. Uncertainty in the Modeling Assumptions

Different types of finite element modeling assumptions were also used. Structural models have been built up by using frame elements and shell elements separately. The properties of the model built up shell elements were presented previous section.

Table 4.3 presents the $1^{st}$ period values of model built up shell and frame elements. The difference between two values is 2.25%.

Table 4.3. $1^{st}$&$2^{nd}$ Period Values Obtained for the Model Built up Shell and Frame Elements.

| $1^{st}$ Period (Beam Model) | $1^{st}$ Period (Shell Element Model) |
|---|---|
| PERIOD (sec) | PERIOD (sec) |
| TS500 | TS500 |
| E=31800 | E=31800 |
| 1.274 | 1.246 |

On the other hand, in order to include the influence of soil conditions, a model including a foundation with soil springs was built up. Soil springs are assigned to the points of the mesh beneath foundation. Soil spring values were calculated by multiplying the subgrade modulus of soil with unit area. Besides, another model that soil layers were represented by solid elements was built up. There are two layers under the foundation presented as in Figure 4.2. The properties of soil layers were tabulated and presented in Table 4.4.

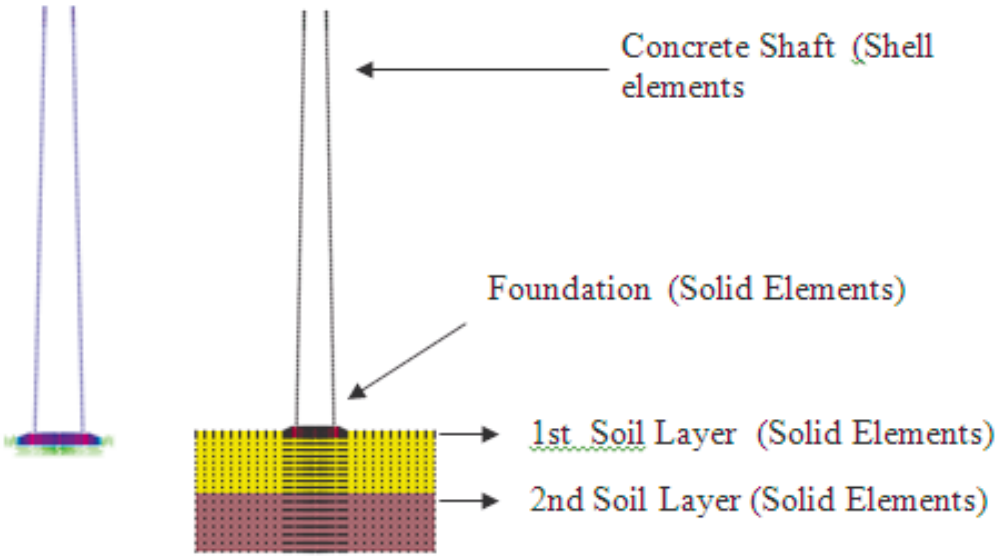


Figure 4.2. Finite Element Models (FEM) of the Chimney that Soil Conditions are Represented by Using Different Modeling Assumptions.

Shear modulus and elastic modulus were calculated by using equations

$$G = \rho {V_s}^2 \tag{4.4}$$

where $\rho$ is specific density of soil,$V_s$ is shear velocity

$$E = 2G(1 + \upsilon) \tag{4.5}$$

Table 4.4. Properties of Soil Layers.

| Soil Type | Height (m) | Shear Velocity (m/s) | Specific Weight (kN/m$^3$) | Poisson Ratio | Shear Modulus (kN/m$^2$) | Elastic Modulus E (kN/m$^2$) |
|---|---|---|---|---|---|---|
| Soil Layer 1 | 15 | 300 | 16 | 0.45 | 144000 | 417600 |
| Soil Layer 2 | 15 | 600 | 22.4 | 0.35 | 806400 | 2177280 |

Soil spring forces assigned beneath the foundation were also calculated by using the formula

$$q_{\lim 1} = \rho v_{s1} \tag{4.6}$$

$$k_{soil} = 40 q_{\lim 1} \tag{4.7}$$

where is the $k_{soil}$ represents the soil spring force and was founded as 20000 kN/m. The $1^{st}$ period values for soil spring model and soil solid model were obtained separately and presented as in Table 4.5.

Table 4.5. $1^{st}$ Period Values Obtained for Different Modeling Assumptions for Soil.

| 1st Period (sec)-Shell Model | 1st Period (sec)-Shell Model |
|---|---|
| Foundation Solid Elements | Foundation Solid Elements |
| ksoil=20000 | 1.91 |
| 1.85 | |

Table 4.6 points out that there are two separate values which were obtained by using different modeling assumptions. For soil spring model $1^{st}$ period was found as 1.85 sec. and for soil solid element model it was also found as 1.91 sec. Comparing those results with fixed supported model, $1^{st}$ period values were higher 48.4%, 53.4% than fixed supported model, separately. That is to say, modeling assumptions have a remarkable effect on the calculation of the period values.

### 4.4. Sensitivity Analysis for Selecting of Updating Parameters

Uncertainties in material properties and modeling assumptions can affect the dynamic properties of the structure. Therefore, sensitivity analysis was carried out in order to determine parameters influencing the first period value of the chimney. These parameters are Young's Modulus of concrete, soil spring coefficient and additional mass due to refractory brick liner. Initial value of Young's Modulus was computed in accordance with American Concrete Institute (ACI) Code (ACI 318, 2008). It is 25743 MPa for C30 concrete class. This value is computed by using design strength compressive strength of concrete $f'_c$. Any records or experimental results of specimen taken during construction phase were not obtained. Therefore, a mean value of $f'_{cm}$ which is calculated by using Equation 4.8 was not identified in accordance with experimental results done on site.

$$f'_{cm} = f'_c + \Delta\sigma \tag{4.8}$$

Besides, $\Delta\sigma$ which is standard deviation value is assumed practically in accordance with some literature as 6 MPa (Ersoy *et al.*, 2001). Thus $f'_{cm}$ value is calculated as 36 MPa for C30 concrete class.

As for the estimation of Young's Modulus value, there are many constitutive concrete models proposed by authors. One of them can be considered as an initial point for estimation of Young's Modulus value. Chang and Mander (1994) proposed the uniaxial hysteretic constitutive model developed (Figure 4.3).

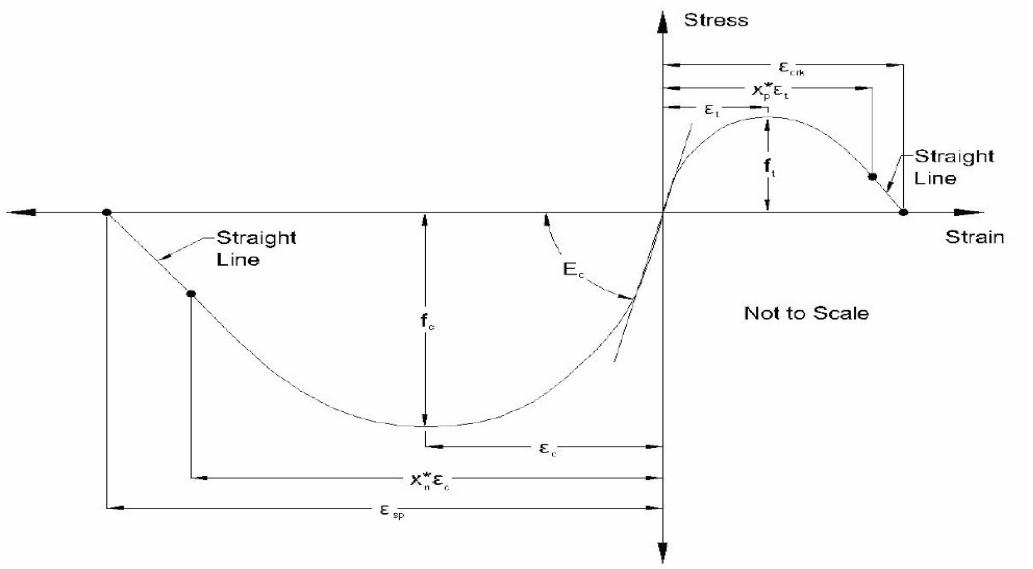


Figure 4.3. Chang and Mender Model.

In accordance with this approach, initial value of Young's Modulus is calculated as indicated in Equation 4.9.

$$E_c = 8200(f'_c)^{3/8} \tag{4.9}$$

The initial value of Young's Modulus can be estimated as 31436 MPa using Chang and Mander's equation from compression test data on concrete cylinder specimens for an mean compressive strength value of approximately 36 MPa. In order to maintain compatibility in terms of using equations to develop demand and capacity distribution, Young's modulus for low level vibration problems is selected as expressed above in accordance with ACI 307-08.

The vertical soil spring coefficient was taken as 20000 kN /m in accordance with soil site investigation report. Vertical springs are assigned to the points of the mesh beneath foundation to represent soil conditions along the vertical direction. Horizontal springs are also assigned to the points of the mesh around the perimeter of foundation to represent lateral conditions of backfill. This value is considered to be as half value of vertical coefficient (Bowles, 1988). Total additional mass due to liner were calculated 340 tons along the height of the chimney. FEMs were built up considering 10 %

decreased and increased values of each parameter. Figure 4.4 presents the effect of parameters on the first period value of the chimney.

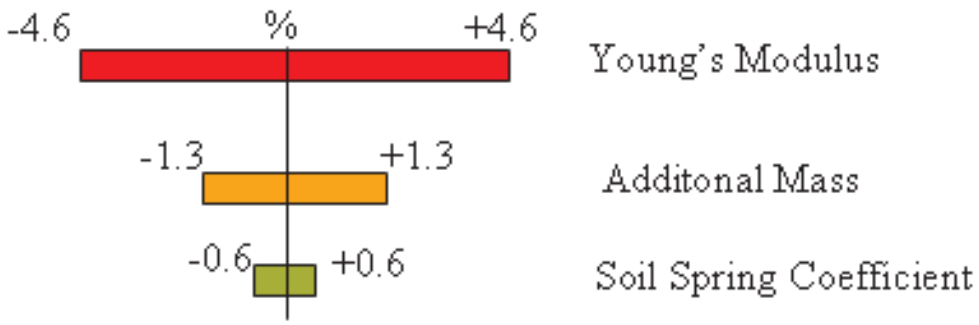


Figure 4.4. Sensitivity Histogram Chart for the Parameters Affects the First Period Value of the Chimney.

Updating parameters were selected as Young's Modulus and soil spring coefficient value. In the light of experiences in construction of the chimney and engineering judgments, any change in the value of mass is not expected. Therefore, additional mass due to refractory brick was not included in updating parameters. Although soil spring coefficient has the smallest effect comparing with other parameters, uncertainty in the soil spring coefficient itself is much larger than the other two parameters. Therefore, it was chosen as one of the updating parameters.

## 4.5. Modal Assurance Criterion - MAC

The Modal Assurance Criterion (MAC) is a statistical indicator of the coherence of two vectors that is it tells how much two vectors resemble. Although this method is mainly used to estimate the coherence of different modes within the same model, the procedure can be used for any two vectors. The MAC of two mode shapes and is calculated by

$$MAC = \frac{|\varphi_A^T \varphi_B|^2}{(\varphi_A^T \varphi_A).(\varphi_B^T \varphi_B)} \tag{4.10}$$

The MAC of two vectors is a scalar and takes a value between 0 and 1, depending on how the vectors are correlated. The MAC is also used to pair matching mode shapes from two different sources, e.g. experimental modes and mode from a FE model.

## 4.6. Model Updating

An error function was generated to minimize the difference between modal parameters obtained from experimental and finite element model results. Error value was obtained by changing values of updating parameters in initial FEM. Modal frequencies and mode shapes were obtained and compared with the ones obtained from system identification results. Optimum values of updating parameters that minimizes error function were found. Equation 4.11 defines error function between measured and simulated modal parameters.

$$E = \sum \left( k_i \left[ \frac{(f_i^* - f_i)}{f_i^*} \right]^2 + h_i [1 - MAC_i]^2 \right) \tag{4.11}$$

where is the $i$ is mode number, is the $k_i$ weighting coefficient for $i^{th}$ modal frequency, is the $h_i$ weighting coefficient for $i^{th}$ modal assurance criteria, is the $f_i^*$ measured modal frequency of $i^{th}$ mode, is the $f_i$ simulated modal frequency of $i^{th}$ mode, is the $MAC_i$ modal assurance criteria for $i^{th}$ mode.

The modal assurance criteria (MAC) were calculated to evaluate the correlation between mode shapes obtained from system identification results and the FEM simulation. Figure 4.5 shows MAC values between FEM modes and experimental ones. The first and second modes are more correlated each other with than compared with the third one.

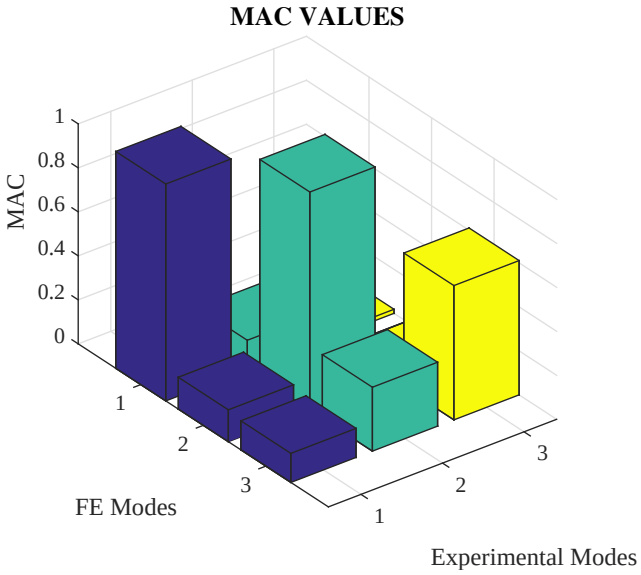


Figure 4.5. MAC Histogram.

Weighing coefficients for the first, second, and third modes were selected based on modal participation ratios that are 67, 26, and 7%, respectively. Initial Young's modulus of concrete was calculated as 25743 MPa and soil spring coefficient was taken as 20000 kN /m. Initial Young's modulus value of 31348 MPa using Chang and Mander equations is not taken into consideration in this study. Demand distribution is developed in accordance with equations written in ACI 307-08 code requirements. Therefore, thee initial Young's modulus value is taken in accordance with ACI 307-08 in order to maintain compatibility in equations used in both demand and capacity distribution. Updated values of Young's modulus of concrete and soil spring coefficient is presented in Table 4.6.

Table 4.6. Values of Updating Parameters.

| UPDATING PARAMETERS | non-updated | updated |
|---|---|---|
| Soil Spring Coefficient (kN/m) | 20000 | 19900 |
| Young's Modulus( kN/m$^2$) | 25743000 | 25642960 |

Table 4.7 shows the vibration frequencies of updated, non-updated FEM and modal identification.

Table 4.7. Identified, Non-Updated And Updated Modal Frequencies.

| Mode Number | Frequencies of Vibration (Hz) | | |
|---|---|---|---|
| | Non Updated FEM | Updated FEM | Modal Identification |
| 1 | 0.55 | 0.59 | 0.59 |
| 2 | 2.46 | 2.69 | 2.54 |
| 3 | 6.03 | 6.54 | 6.01 |

Furthermore, Figure 4.6 illustrates the first, second and third mode shapes of identified, updated FEM and non-updated FEM.

Consequently, identified modal parameters of first mode and second mode are well represented in updated FEM due to the fact that modal participating ratios have are higher values for the first two modes.

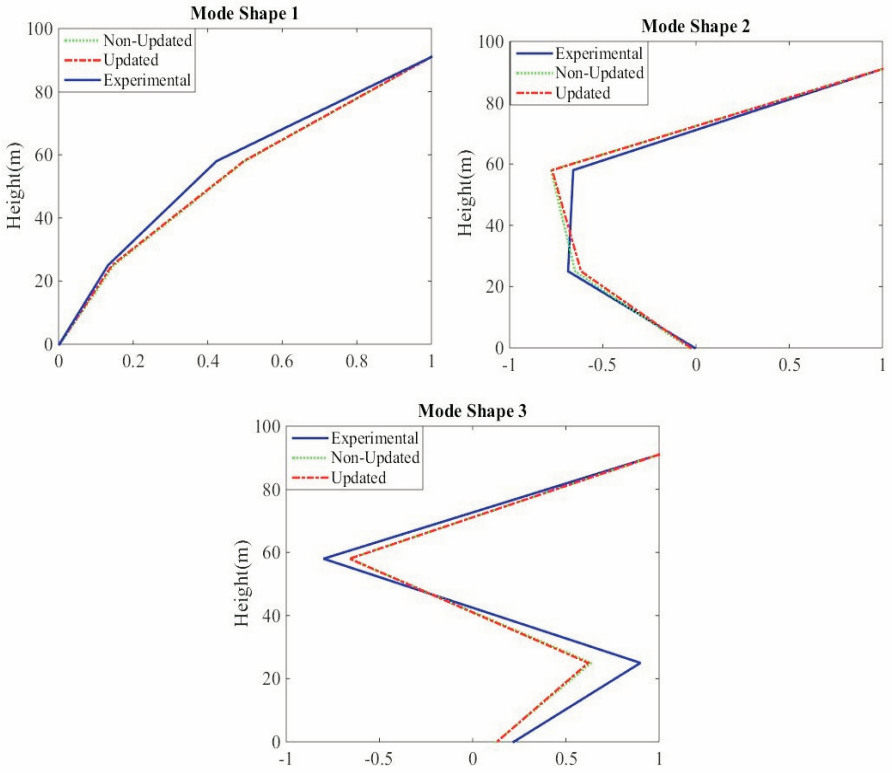


Figure 4.6. Experimental, Updated and Non-Updated Mode Shapes.

# 5. EARTHQUAKE LOADING

## 5.1. Probabilistic Seismic Hazard Analysis (PSHA)

Assessment of the chimney was performed based on probabilistic approaches. Therefore, probabilistic seismic hazard analysis was carried out to develop demand distribution of chimney under earthquake loading. For this reason, a possible earthquake scenario in Marmara Region, Turkey was considered. In accordance with this scenario, the assumption that a larger magnitude earthquake occurring far from site and moderate earthquake occurring close to the site was made. Earthquake ground motion includes uncertainties due to location, size and attenuation relationships. Therefore, the goal of Probabilistic Seismic Hazard Analysis (PSHA) is to determine probability of occurrence of an event exceeding a demand level within a period considering these uncertainties. PSHA gives the intensity measure for the site in probabilistic terms. This was basis for selecting earthquake records in order to develop demand distribution.

## 5.2. Assumptions made for PSHA

The framework of the PSHA was established by Cornell (1968). The classical well-known PSHA method is further developed as Cornell-McGuire PSHA (McGuire, 1995). In accordance with this approach (McGuire,1995, Kramer, 1996), probability of exceedance of an event, at least once in a given time span, and at a given site, a set of ground motion parameter levels can be calculated by the formula given in Equation 5.1.

$$P(X \geq x|\, T) = \sum_{i=1}^{I} \upsilon_i(m) f_i(R|\, m) P(X \geq x|\, m, R) dR dm \tag{5.1}$$

where $\upsilon_i$ is the activity rate of the sources.
This classical approach includes four main steps which are:

- Definition of sources: The types of the sources may range from small planar

faults to large seismotectonic provinces. This can be defined as point, line or area sources.

- Recurrence Relationship: Each source is characterized by an earthquake probability distribution or simply by a recurrence relationship in probabilistic analyses. The temporal distribution of earthquake recurrence is called a recurrence relationship, which specifies the average rate at which an earthquake of some magnitude will be exceeded.

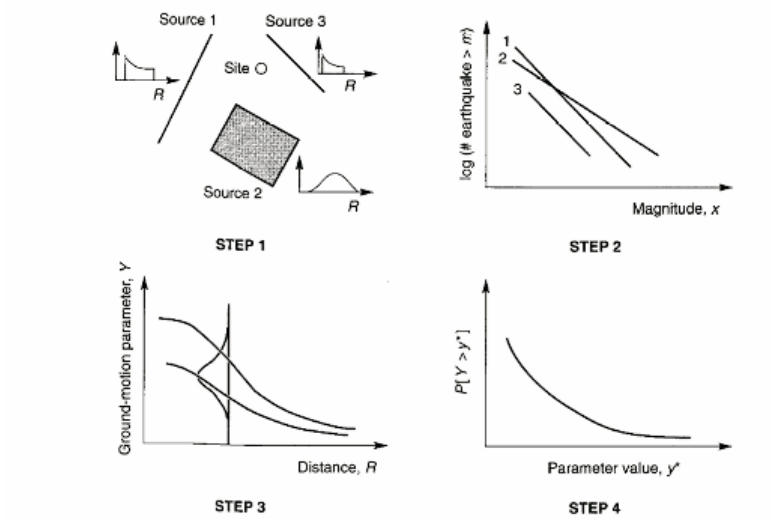


Figure 5.1. Steps of Classical PSHA Approach (Kramer, 1996).

- Determination of ground motions: Ground-motion intensity measures (such as spectral accelerations) produced at the site by earthquakes of any possible magnitude, occurring at any possible point in the source zone, using ground-motion prediction equations are obtained.

- Hazard calculation: The hazard curves which indicate probability of exceedance of an event, at least once in a given time span, and at a given site, a set of ground motion parameter levels are developed.

Classical approach was improved by Field (Field *et al.*, 2003) by combining earthquake-rupture forecasts, ground-motion models. Validation of improved PSHA

approach was made again by the same authors (Field *et al.*, 2005). Open source software applications were developed depending on the recent improvements (OpenSHA, www.opensha.org).

Furthermore, new contributions have been introduced to enhance boundaries of applications (Monelli *et al.*, 2014) and a new software application has been presented (OpenQuake, http://www.globalquakemodel.org/openquake/about/).
All these follow the same assumptions that;

- Seismicity is generated by a set of independent seismic sources (probability of occurrence of an event in a source is independent an event generated by other sources).This can be summarized as in Equation 5.2.

$$\begin{aligned} &P(X \geq x|\, T) = 1 - P_{src1}(X < x|\, T) * P_{src2}(X < x|\, T)...P_{srcI}(X < x|\, T) \\ &= 1 - \prod_{i=1}^{I} P_{srci}(X < x|\, T) \end{aligned} \tag{5.2}$$

- Earthquakes generated by a seismic source are independent. This is illustrated in Equation 5.3.

$$\begin{aligned} &P_{srci}(X < x|\, T) = P_{rup1}(X < x|\, T) * P_{rup2}(X < x|\, T)...P_{rupN}(X < x|\, T) \\ &= \prod_{j=1}^{N} P_{rupj}(X < x|\, T) \end{aligned} \tag{5.3}$$

- Earthquakes follow a Poissonian distribution. This is shown in Equation 5.4.

$$P_{rupj}(k|\, T) = e^{-\upsilon_j T} \frac{(\upsilon_j T)^k}{k!} \tag{5.4}$$

The final equation can be rewritten as in Equation 5.5.

$$P(X \geq x|\, T) = 1 - e^{-\sum_{i=1}^{I}\sum_{j=1}^{N_i} \upsilon_j T * P(X \geq x|rupij)} \tag{5.5}$$

## 5.3. Earthquake Scenario

Marmara region is a territory that has high risk for seismic activity and it covers the largest area of industrial facilities in Turkey. A reasonable earthquake scenario was defined considering multiple ruptures of the Islands, Mid-Marmara, and Off-Tekirdag fault segments. (Gulkan, 2012).These segments are far from site and generate larger magnitude earthquakes. Furthermore, another segment, Bilecik fault is close to site and it was considered to generate moderate size earthquake. Figure 5.2 illustrates plausible scenario in the region. In the figure, star signs represent the location of hypocenter of faults.

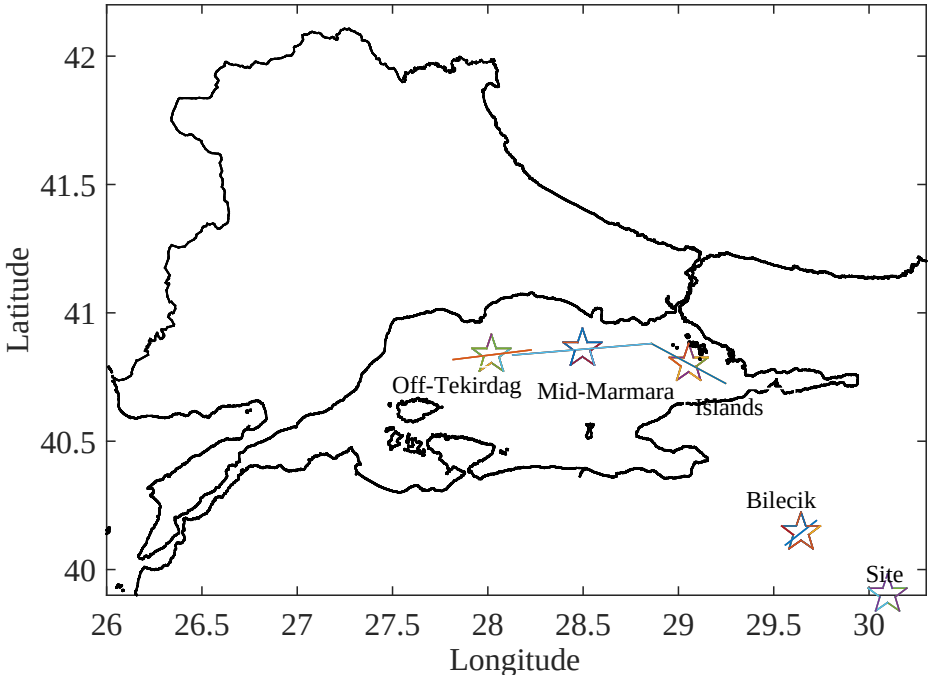


Figure 5.2. Faults Segmentation and Site Location.

Rupture length (RL) and characteristic magnitudes (Mc) was calculated in ac-

cordance with magnitude scaling relationship given Wells and Coppersmith (1994).The basic formula is defined in Equation 5.6.

$$M_C = 5.08 + 1.16 \log(RL) \tag{5.6}$$

Table 7.1 presents The properties of faults used in PSHA calculation. Selected fault

Table 5.1. The Properties of Faults Used in PSHA Calculation.

| Fault Name | Slip Rate(mm) | Rupture Length (km) | Mchar |
|---|---|---|---|
| Off-Tekirdag | 23 | 51 | 7.1 |
| Mid-Marmara | 23 | 62 | 7.2 |
| Islands | 23 | 51 | 7.1 |
| Bilecik | 20 | 17 | 6.08 |

segments were assumed to rupture in strike-slip mechanism along their entire length (Kalkan *et al.*, 2009).

### 5.4. Fault Modeling Involving a Recurrence Equation

Faults were modeled depending on fault geometries. Epistemic uncertainties based on geological characteristics type such as slip rate, magnitude scaling relationship were considered by using a Youngs & Coppersmith (1985) characteristic recurrence model. Magnitude frequency relationship was developed for all faults depending on the simple moment balance with the total moment release rate (in Nm) on the fault. Total moment rate was calculated in accordance with Equation 5.7 (Andersen and Luco, 1983).

$$\dot{M}_o = \mu A \, \dot{s} = \upsilon \int_{M_{\min}}^{M_{\max}} f_m(M_w) M_o(M_w) dm \tag{5.7}$$

Where $\mu$ is shear modulus of the ground in Pa, A ($km^2$) is the area of the fault, s is annual slip rate of the source (mm), is activity rate of seismic source, $f_m(M_w)$)

represents magnitude frequency distribution. Seismic moment $M_o(M_w)$ was computed given in Equation 5.8 (Hanks and Kanamori, 1979).

$$M_o(M_w) = 10^{16.05+1.5M_w} \tag{5.8}$$

The Youngs and Coppersmith recurrence model follows an exponential distribution for lower magnitudes and a fixed recurrence rate for the characteristic magnitude. This can be expressed in Equation 5.9.

$$\begin{aligned} N(M) - N(M_c) &= \frac{\mu A \dot{s} e^{(-\beta(M_{MAX}-M-0.5))} M_o^{MAX}}{1-e^{(-\beta(M_{MAX}-M-0.5))}} \left[\frac{b10^{-c/2}}{c-b} + \frac{be^{\beta}(1-10^{-c/2})}{c}\right] \\ N(M_c) &= \frac{\beta(N(M)-N(M_C))e^{-\beta(M_{MAX}-M-1.5)}}{2(1-e^{-\beta(M_{MAX}-M-1.5)})} \end{aligned} \tag{5.9}$$

Where c=1.5 and $\beta = bln(10)$ and $b$ value is calculated as 0.70 for the seismic area defined in earthquake scenario.

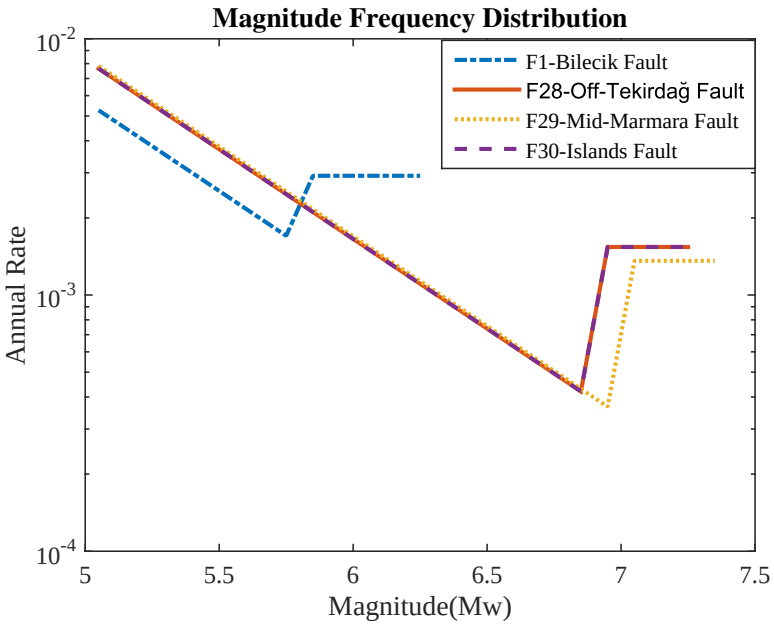


Figure 5.3. Magnitude Frequency Distribution Corresponding Faults.

Magnitude frequency distribution corresponding faults were obtained and presented in Figure 5.4.

## 5.5. Hazard Calculations

Seismic hazards curves were obtained for an earthquake which has 10% probability of exceedance in 50 years (CICIND, 2001). Ground motion prediction equation (GMPE) of Akkar *et al.*, (2014) was selected to represent the ground motion variability in the selected area.

As for rupture scenario in faults, a rupture floating model which manages how partial ruptures are floated across a fault source surface was defined. All possible rupture locations were simulated along both dip and strike directions. Firstly, upper and lower seismological layer bounds of faults were determined. Afterwards, rupture width and length were calculated in for earthquake magnitude levels to be considered in hazard calculations. Furthermore, fault rupture dimensions can vary along both dip and strike directions under an earthquake event (Dowrick and Rhoades, 2004). For this reason, earthquake ruptures should be scaled by an aspect ratio (Leonard, 2010). In this study, distance uncertainty is not taken into consideration for the simplicity of calculation. In order to include soil condition, Vs30, shear velocity of soil for given site was taken as 300 m/sec.

Eventually, hazard curves were obtained for given site. Hazard curves for T=1.80 sec and T=0.40 sec which belongs the first and second period value of chimney for updated FEM were presented in Figure 5.4. Deaggregation analysis was carried out to investigate relative contribution of earthquake sources to the total probability of exceedance of a certain ground motion level at a given site (Bazzurro and Cornell, 1999). Deaggregation in terms of $\varepsilon$ was also obtained for the contribution of different ground motion distributions. This is expressed simply as:

$$\varepsilon = \frac{x - \mu}{\sigma_{total}} \tag{5.10}$$

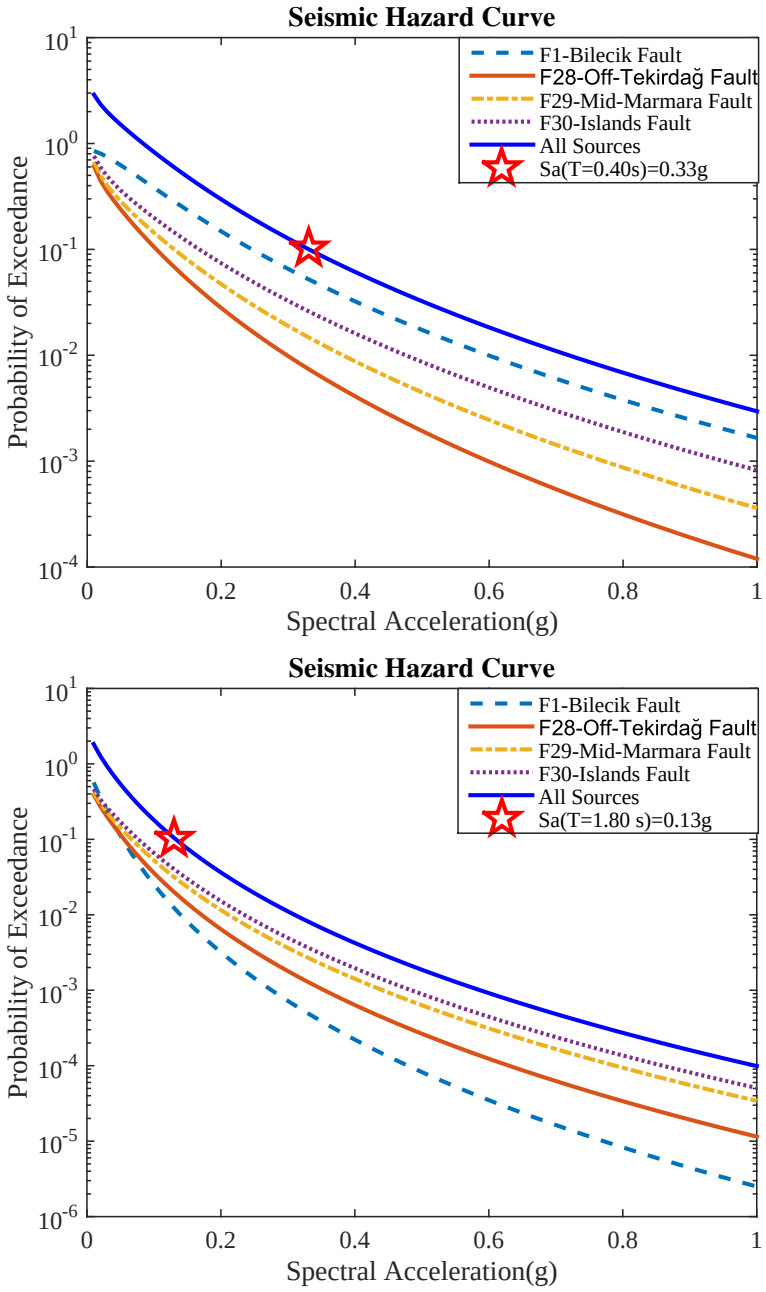


Figure 5.4. Contribution to Hazard by Sources T=1.80 sec and T=0.40 sec for 10% Probability of Exceedance in 50 years for the Site of Chimney.

Where $x$, intensity ground motion level, was selected as spectral acceleration in this study,$\mu$ mean value of intensity ground motion level calculated by GMPE and standard deviation $\sigma_{total}$ term includes inter and intra events. Deaggregation results were also presented for each period value written above in Figure 5.5.

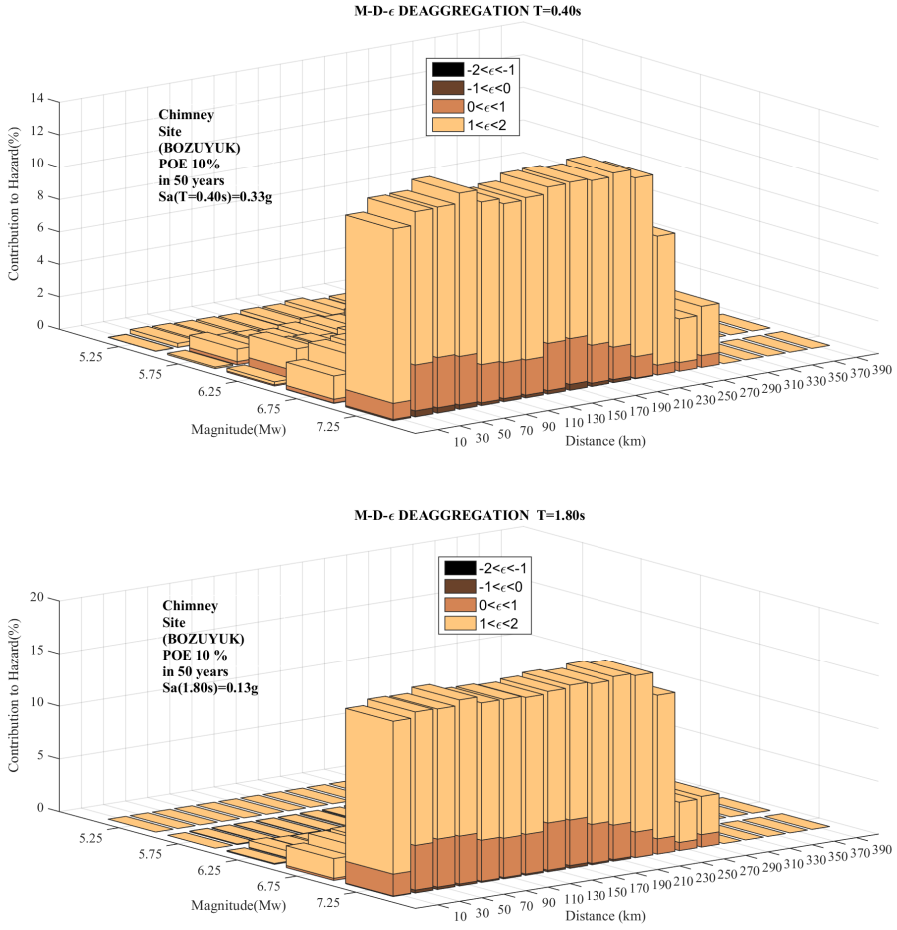


Figure 5.5. Deaggregation results T=1.80 sec and T=0.40 sec for 10% Probability of Exceedance in 50 years for the site of Chimney.

Aside from them, seismic hazard maps were generated in order to see hazard propagation globally for selected earthquake scenario. Similarly, the results were obtained and shown in Figure 5.6 for 10% probability of exceedance in 50 years for the site of chimney.

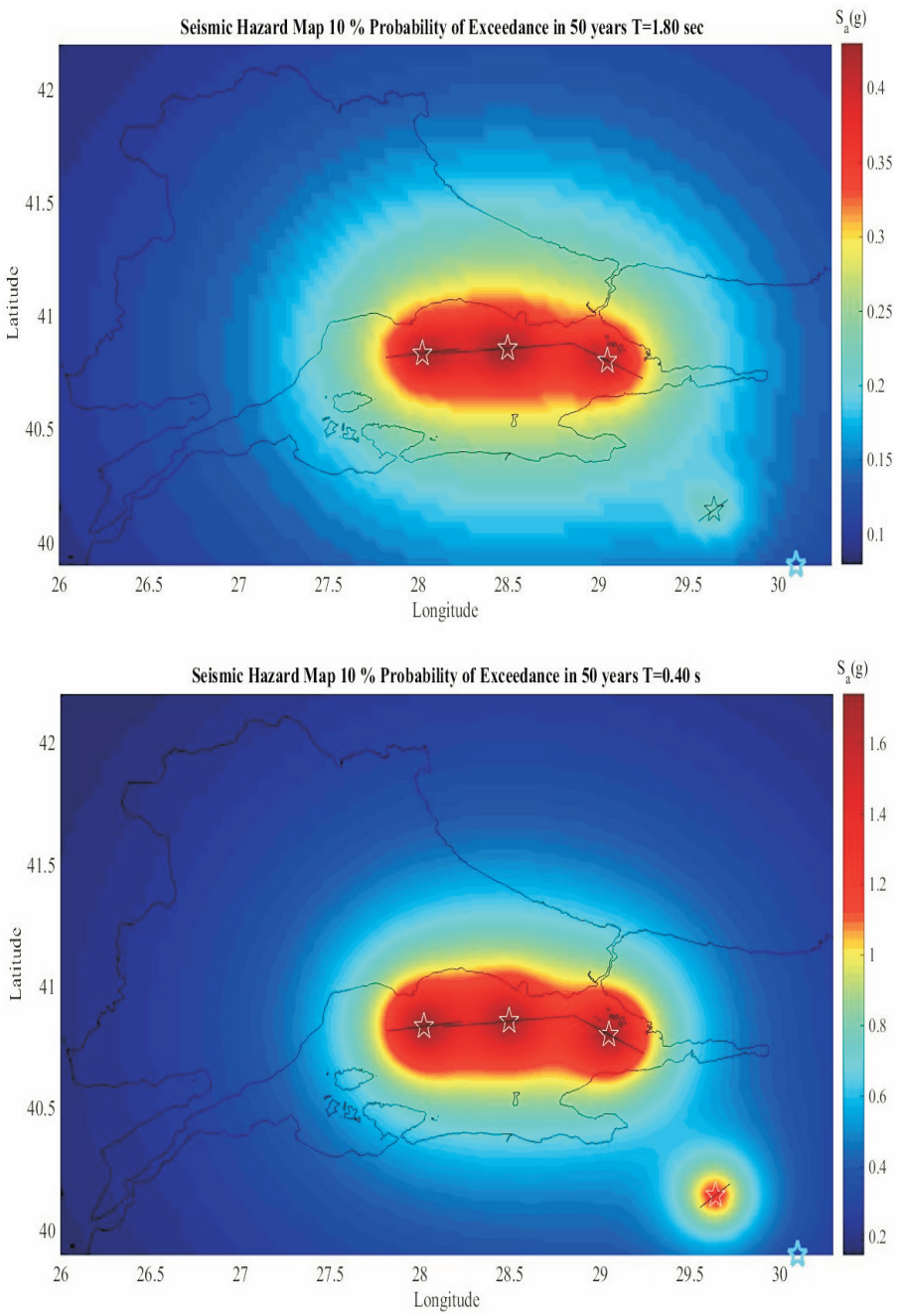


Figure 5.6. Seismic Hazard Maps Generated T=1.80 sec and T=0.40 sec for 10% Probability of Exceedance in 50 years for the site of Chimney.

Consequently, uniform hazard spectrum (UHS) was developed by calculating spectral acceleration values for many periods in the range of interest for the hazard level that has 10% probability of exceedance in 50 years. This was presented in Figure 5.7.

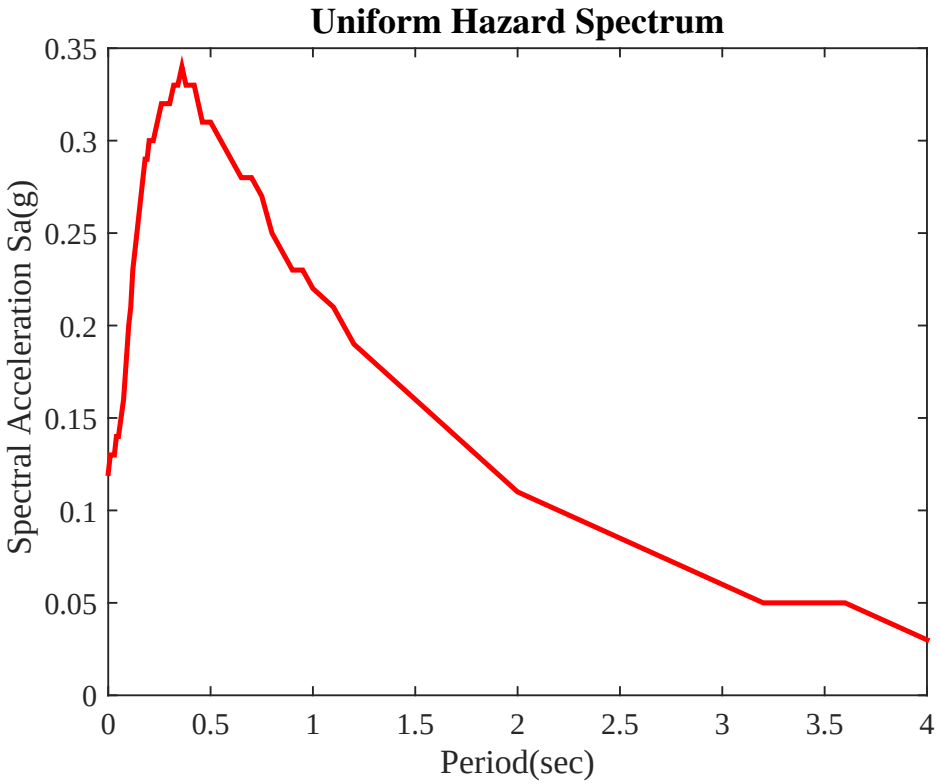


Figure 5.7. Uniform Hazard Spectrum (UHS) Developed for 10% Probability of Exceedance in 50 years for the site of Chimney.

As a result of hazard calculations, the trend of the deaggregation results with spectral periods indicates that the probability exceedance of long-period spectral accelerations is controlled by earthquakes that are larger in size and farther from the site than those governing short-period spectral acceleration values. Major contribution to the hazard in terms of distance was found 70 -100 km. Events with magnitude ranging from 7.0 to 7.5 has the most contribution to the hazard for 10% probability of exceedance in 50 years (Equation 5.10). This information was basis for generating demand distribution for reliability estimation.

# 6. WIND LOADING

## 6.1. Wind Simulation By Using Multivariate Stochastic Process

Wind field can be simulated as a stochastic process. Wind velocity comprises two parts. These are mean and fluctuation (gust) part. In this study, the fluctuation part was simulated as a Gaussian ergodic stationary multivariate stochastic process. Wind load affects the chimney as pressure distribution along the height. Linear time history analysis of the chimney under wind load was carried out for reliability estimation.

## 6.2. Mean Wind Profile and Characterization

Wind field can be characterized by mean velocity profile and can be modeled as a stochastic stationary Gaussian process. Wind velocity can be defined as in Equation 6.1 (Simiu and Scanlan, 1996).

$$U(z,t) = \bar{U}(z) + u(z,t) \tag{6.1}$$

where is the $U(z,t)$ wind velocity, is the $\bar{U}(z)$ mean velocity at height $z$, is the $u(z,t)$ fluctuation velocity at height $z$.

Wind profile along the height of the chimney was developed by using logarithmic law. Mean wind velocity profile was expressed as in Equation 6.2

$$U(z) = \frac{1}{k} u_* \ln \frac{z}{z_o} \kappa = \frac{k}{\ln(10/z_o)} u_* = \sqrt{\frac{\kappa}{{V_b}^2}} \tag{6.2}$$

where is the $k$ von karman constant, equal to 0.4, is the $z_0$ terrain toughness taken as 0.03 for the location of open terrain, is the $z$ the height, is the $u_*$ shear velocity, is the $\kappa$ surface drag coefficient.

In order to generate wind data, the basic wind speed, the mean velocities mea-

sured at 10 m above the ground in 10 min period which has probability of exceedance at least once in 50 years, was taken as $V_b$ =30 m/sec in accordance with wind report given by local administration.

### 6.3. Simulation of Wind Velocity Fluctuation Fields

Wind velocity fluctuation fields were simulated by using multivariate stochastic process. The spectral representation method first proposed by Shinozuka and Jan, (1972). Shinozuka (1974) used Fast Fourier Transform (FFT) technique to reduce computation time drastically. Furthermore, Li and Kareem (1991) used FFT technique to generate multivariate stochastic process. Deodatis and Shinozuka (1989) developed a technique to simulate stochastic waves. Shinozuka *et al.*, (1989) built a method to simulate ergodic multivariate stochastic processes by using the concept of double-indexing the frequencies. However, sample functions simulated by using this technique were not ergodic. Later, the spectral representation method was further developed by Deodatis (1996) and was used to successfully simulate ergodic multivariate stochastic processes.

In accordance with the methodology, a set of *m-variate* homogenous Gaussian one dimensional processes (1-D) $f_j^0(x)(j = 1, 2, ..m)$ with mean zero and with the cross-spectral density matrix $S^o(w)$ defined by

$$S^o(w) = \begin{bmatrix} S_{11}^0(w) & S_{12}^0(w) & ..... & S_{1m}^0(w) \\ S_{21}^0(w) & S_{22}^0(w) & .... & S_{2m}^0(w) \\ .... & ..... & ..... & .... \\ S_{m1}^0(w) & S_{m2}^0(w) & & S_{mm}^0(w) \end{bmatrix} \tag{6.3}$$

Multivariate stochastic functions were simulated by using Equation 6.4.

$$f_j{}^o(t) = 2 \sum_{m=1}^{j} \sum_{l=1}^{N} H_{jm}(\omega_{ml}) \sqrt{\Delta w} \cos\left[\omega_{ml} t - \theta_{jm}(\omega_{ml}) + \varphi_{ml}\right] \tag{6.4}$$

where $j = 1, 2, 3, ...n$ and $H_{jm}$ is a element of a lower-triangular matrix $H(\omega)$, which

can be obtained a Cholesky decomposition of the cross-spectral density matrix $S(\omega)$ that is,

$$S^o(w) = H(w).\bar{H}(w)^T \tag{6.5}$$

$H_{jm}$ can be expressed as in Equation 6.6

$$H_{jm}(\omega_m) = |H_{jm}(\omega_m)| \exp(i\theta_{jm}(\omega)) \tag{6.6}$$

where $i^2 = -1$ and

$$\theta_{jm}(\omega) = \tan^{-1}\left(\frac{\mathrm{Im}\left(H_{jm}(\omega)\right)}{\mathrm{Re}\left(H_{jm}(\omega)\right)}\right) \tag{6.7}$$

The double-indexing the frequencies is expressed by

$$\omega_{ml} = (l-1)\Delta\omega + \frac{m}{n}\Delta\omega \tag{6.8}$$

where $\Delta\omega$ is defined as

$$\Delta\omega = \frac{\omega_u}{N} \tag{6.9}$$

$\omega_u$ is upper cutoff frequency beyond which the elements of the cross-spectral density matrix, $N$ is amount of frequency range. In Equation 6.10 $\phi_{ml}$ represents the random independent phase angles uniformly distributed between 0 and $2\pi$.

By using the advantage of FFT technique, Equation 6.10 can be rewritten in the following form

$$f_j(p\Delta t) = \mathrm{Re}\left\{\sum_{m=1}^{j} h_{jm}(q\Delta t) \exp\left[i\left(\frac{m\Delta\omega}{n}\right)(p\Delta t)\right]\right\} \tag{6.10}$$

Where $p = 0, ....nM - 1 j = 1, ....n$ and,

$$h_{jm}(q\Delta t) = \sum_{l=0}^{M-1} B_{jm}(l\Delta\omega) \exp(i(l\Delta\omega)(q\Delta t)) \tag{6.11}$$

where $q$ is the remainder of the division of $p$ and $M$ with

$$B_{jm}(l\Delta\omega) = \begin{cases} \sqrt{2\Delta\omega}\,|H_{jm}(\omega_{ml})| \exp(-i\theta_{jm}(\omega_{ml}) \exp(i\varphi_{ml}), 0 \leq l \leq N-1 \\ 0, N \leq l \leq M-1 \end{cases} \tag{6.12}$$

Sampling period and the period of simulation function is calculated as

$$\Delta t = \frac{2\pi}{M\Delta\omega}, T_0 = \frac{2\pi nN}{\omega_{up}} \tag{6.13}$$

$h_{jm}$ can be computed by inverse Fourier transform of $B_{jm}$. On the other hand, the elements of $S^o(w)$, spectral density matrix are found

$$S_{jk}(\omega) = \sqrt{S_j(\omega)S_k(\omega)}Coh(\Delta_{jk}, \omega) \tag{6.14}$$

where $j, k = 1, 2, 3, ...n, j \neq k$ and velocity fluctuations are correlated between each other at two different heights $z_j$ and $z_m$. Coherence function developed by Davenport (1968) was used.

$$Coh(\Delta_{jm}, \omega) = \exp\left[-\frac{\omega}{2\pi}\frac{\left[(C_z\Delta z)^2\right]^{1/2}}{\frac{1}{2}\left(U(z_j) + U(z_m)\right)}\right] \tag{6.15}$$

$\Delta_{jm}$ is the distance between two points and $C_z$ is equal to 10 for design purpose. In order to simulate wind fluctuations, ground roughness $z_o = 0.03$, number of frequency $N$= 4096, $\omega_u$= 25$\pi$ rad/sec upper cut-off frequency were defined and $\Delta t$= 0.01 sec and $\Delta\omega$= 0.0383 rad/sec were calculated. Kaimal's spectrum formula given in Equation 6.16 was used and the spectrum was plotted shown in Figure 6.1.

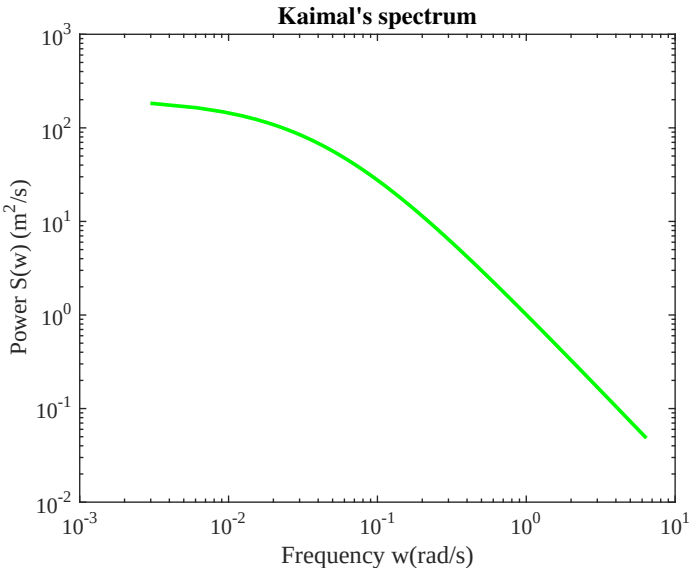


Figure 6.1. Von Kaimal's Spectrum.

Wind velocity fluctuations were simulated along the height of the chimney at 100 points. In this way, the period of the simulated multivariate stochastic process was $T_o$= 409600 seconds.

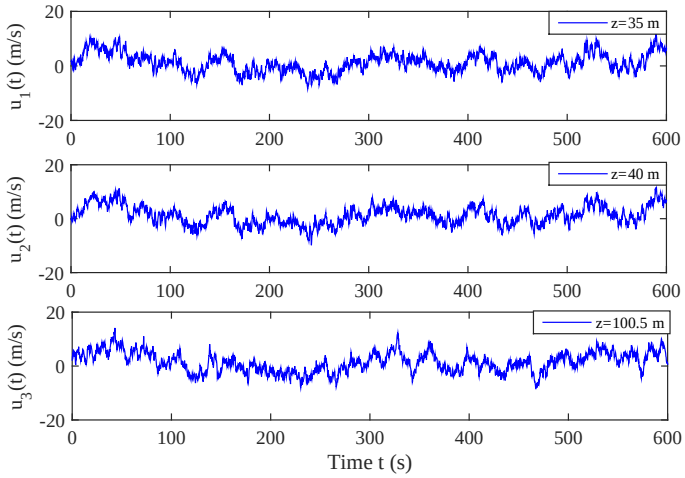


Figure 6.2. Generated Sample Functions for Longitudinal Velocity Fluctuation at three Different Heights, Over the First 600 s of $T_o$.

The results for the first 600 seconds at elevation +35.00 m, +40.00 m and +100.5 m were presented in Figure 6.2. Furthermore, Figure 6.3 presents the auto and cross correlation functions of the realizations at given points of the simulated multivariate

stochastic process. In accordance with the plotted figure, the correlation between elevation +35.00 and +40.00 m are strong since they are close to each other and a weaker correlation was seen between elevation +35.00 and +100.5 m.

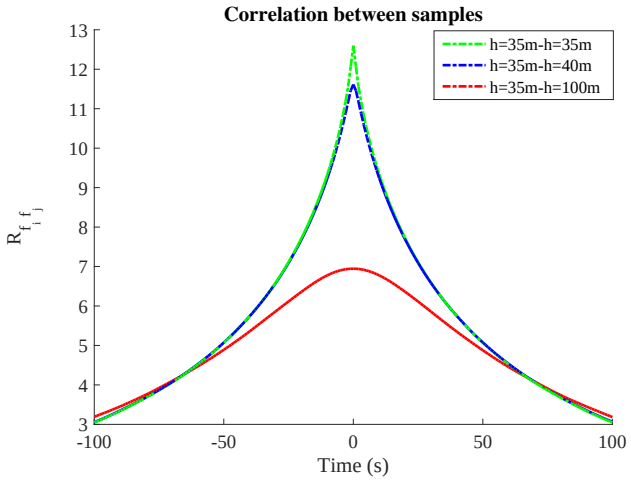


Figure 6.3. Auto and Cross Correlation Functions of Simulated wind Velocity Fields at Elevation +35.00, +40.00 and +100.5.

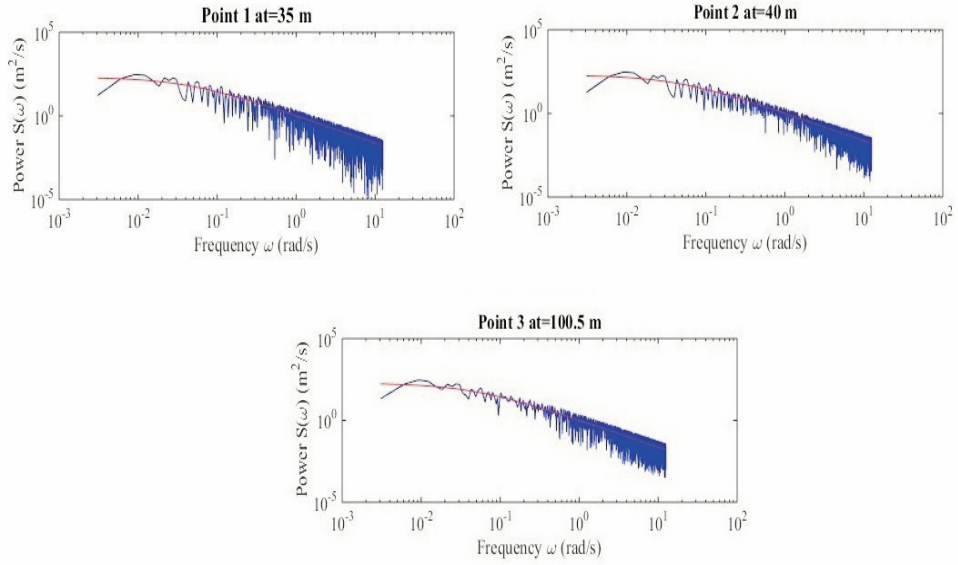


Figure 6.4. Power Spectrum of Generated Sample Functions vs Corresponding Targets.

Figure 6.4 presents the power spectral density check of the simulated wind velocity horizontal fluctuation fields. As can be seen in the figure, simulated spectra were in good match with target spectra.

## 6.4. Along wind Load Actions

Reinforced concrete chimneys are designed to resist the wind forces in both the along-wind and across-wind directions. Acrosswind actions are not primary concern for the chimney because of the fact that the frequency of the chimney is far from the acrosswind frequency. Therefore, acrosswind actions were not calculated in this study. In order to show that power spectral density function of Acrosswind was plotted by using Equation 6.16.

$$S_{CL}(f) = \sigma_{CL}^2 \frac{1}{\sqrt{\pi} B_c f_s} \exp\left[-\left(\frac{1-\frac{f}{f_s}}{B_c}\right)^2\right] \tag{6.16}$$

where $B_c$ band with of the spectrum, is the $f_s$ dominant frequency of vortex shedding, structure frequency, is the $\sigma_{CL}^2$ mean square value of $C_L$ lift coefficient

The frequency of the chimney was calculated as 0.59 Hz and Figure 6.5 presents that frequency of the chimney falls apart from the plateau which acrosswind is effective between 0.7-1.6 Hz.

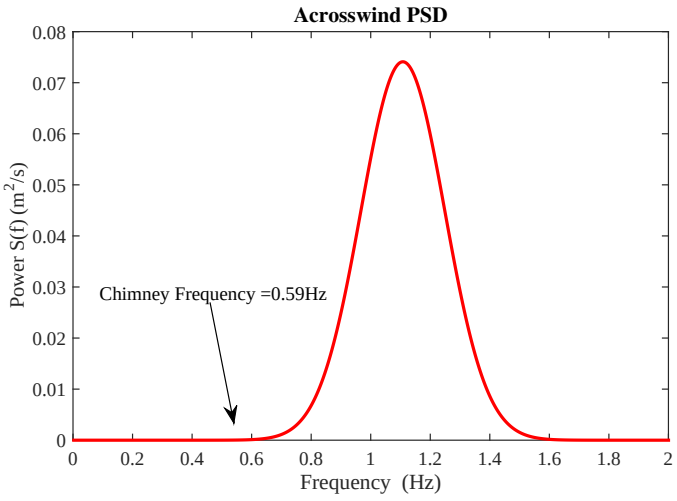


Figure 6.5. Power Spectrum of Acrosswind Action.

In the light of the procedure described above, wind velocity profile was obtained as in Figure 6.6.

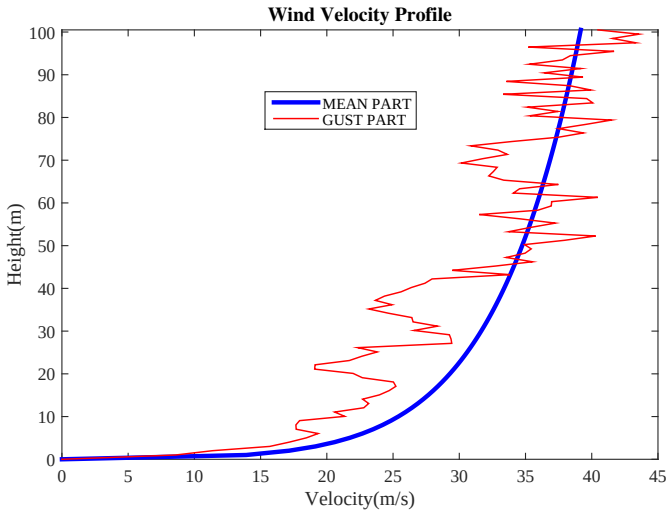


Figure 6.6. Wind Velocity Profile.

For along-wind forces, a "strip" assumption regarding the forces on a section of the structure with the flow condition upstream of the section was applied (Holmes, 2001).

Alongwind aerodynamic actions were calculated by using obtained wind profile as follows:

$$F(z,t) = \bar{F}(z) + f(z,t) \tag{6.17}$$

where, $\bar{F}(z)$ is the wind load value along the chimney height regarding mean part of wind profile defined as in Equation 6.18.

$$\bar{F}(z) = \frac{1}{2}\rho C_d(z) D(z) \bar{U}^2(z) \tag{6.18}$$

and $f(z,t)$ is the wind load value regarding fluctuation part of wind profile expressed as

$$f(z,t) = \rho C_d(z) D(z) \bar{U}(z) u(z,t) \tag{6.19}$$

$C_d(z)$, is the drag coefficient taken as in accordance with (ACI 307-08)

$$\begin{aligned} C_d(z) &= 0.65, for z < z - 1.5d(z) \\ C_d(z) &= 1, for z = z - 1.5d(z) \end{aligned} \tag{6.20}$$

$D(z)$ is the diameter of the chimney section at height $z$.

# 7. RELIABILITY ESTIMATION

Reliability estimation of the chimney under wind and earthquake loading was performed, based on overturning moment at base section of the chimney, separately. The structural performance of the chimney shell in whole or part was assessed in accordance with specified limit states written in codes. CICIND 2001 or 2011 provisions propose two limit states.

- The ultimate limit states which concern the maximum load carrying capacity including overturning of the structure of the structure and reaching the maximum resistance capacity of sections. In this case, the exceedance of a limit state may be reversible or irreversible. In the irreversible case the damage associated with the exceedance will remain until the structure has been repaired. In the reversible case the damage or malfunction will remain only while the cause of the exceedance is present.
- The serviceability limit states which concern the normal use including local damage with excessive cracking which may reduce the durability of the structure or affect the appearance of structural elements. In the cases of permanent local damage the exceedance of a serviceability limit state is irreversible and the first occurrence constitutes failure.

Where the chimneys are the sensitive of tensile stresses due to severe wind and earthquake loading condition, it is important to check the sections under ultimate limit states.

In this study, extreme wind load case was not taken into consideration. The threshold value was considered to be as cracking moment capacity by using serviceability limit state condition under wind loading. Furthermore, threshold value was considered to be yield moment capacity of the section under earthquake loading. If demand value exceeds beyond this threshold limit, the assumption that the failure occurs at the base section of the chimney was made.

## 7.1. Earthquake Loading

Codes of practice for structures generally recognise that it is not economical to design structures to remain elastic at the ultimate earthquake event and generally allow some inelastic behaviour. The seismic design approach described in this section which has been incorporated into the 2001 CICIND code is based on dual performance criteria:

(i) Designing the chimney elastically to resist earthquake induced forces considered reasonable for a serviceability limit state earthquake event (SLS),
(ii) Designing the chimney with sufficient ductility so that the chimney will not collapse when subject to an extreme earthquake event at the structural stability limit state (SSLS).

The serviceability limit state (SLS) is associated with the ultimate strength of the chimney being reached whilst the structural stability limit state (SSLS) is associated with inelastic failure of the chimney. The seismic design approach recommended in CICIND 2001 and ACI307-98 encourages elastic behaviour with no requirements for ductility. The structural response factor is considered to be as R=1 in these codes. Afterwards, 2011 CICIND code provision propose the importance factors and structural response factors as given in the Figure 7.1.

Table 7.1. Importance and Structural Response Factors.

| Class | Detailing | Seismicity | IF | R |
|---|---|---|---|---|
| 1 | Elastic | Low | 1.2 | 1 |
| | | High | 1.2 | 1 |
| 1 | Seismic | Low | 1 | 2 |
| | | High | 1 | 2 |
| 2 | Elastic | Low | 1.4 | 1 |
| | | High | 1.4 | 1 |
| 2 | Seismic | Low | 1.4 | 2 |
| | | High | 1.4 | 2 |

The structural response factor depends on the level of seismic detailing:

- R = 1.0 no specific seismic detailing,
- R = 2.0 seismic detailing ( Capacity Design)

ACI 307-08 code also recommends the chimney to be designed by use the structural response factor as R=1.5.

As for EC8-3, it encourages ductility through the formation of one plastic hinge using capacity design principles. Concrete chimneys may be designed for dissipative behavior with a basic value of the behavior factor R=2.5.

TSC 2007 gives the structure response factor as R=3, however, there is not any information regarding limit states, detailing etc.

Reliability estimation of the chimney based on linear time history analysis with updated and non-updated systems was performed. Demand distribution of the chimney was developed depending on overturning moment values at base of the chimney obtained under selected earthquake records utilizing PSHA results. Capacity distribution of the chimney section was also developed depending on ultimate moment capacity of chimney section at base by using Monte Carlo simulation.

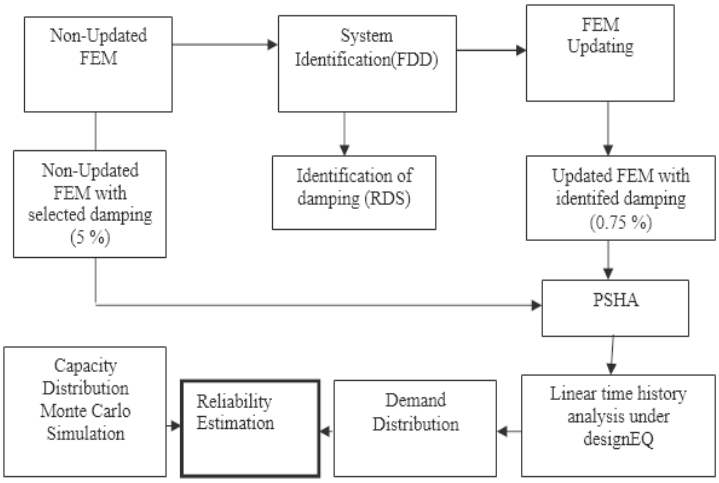


Figure 7.1. The Flowchart that Summarizes All Steps to Estimate Reliability of the Structure Under EQ Loading.

Reliability of the structure was found by using joint probability distribution of demand and capacity curves. Figure 7.1 shows the flowchart that summarizes all steps to estimate reliability of the structure.

### 7.1.1. Development of Demand Distribution

A set of horizontal ground motions were selected from the PEER NGA database and they were scaled to match spectral acceleration of UHS of the site developed in the previous section at the first structural period records matching the target spectrum ($http://peer.berkeley.edu/peer_ground_motion_database$). Figure 7.2 presents response spectra of scaled ground motions matching UHS.

Since the first period value of updated FEM is close that of non-updated FEM, the same ground motion records and the same scale factors were observed. Response spectra of selected twelve ground motion records were plotted for the first period value of updated FEM, T=1.83 sec (Baker and Cornell, 2006).

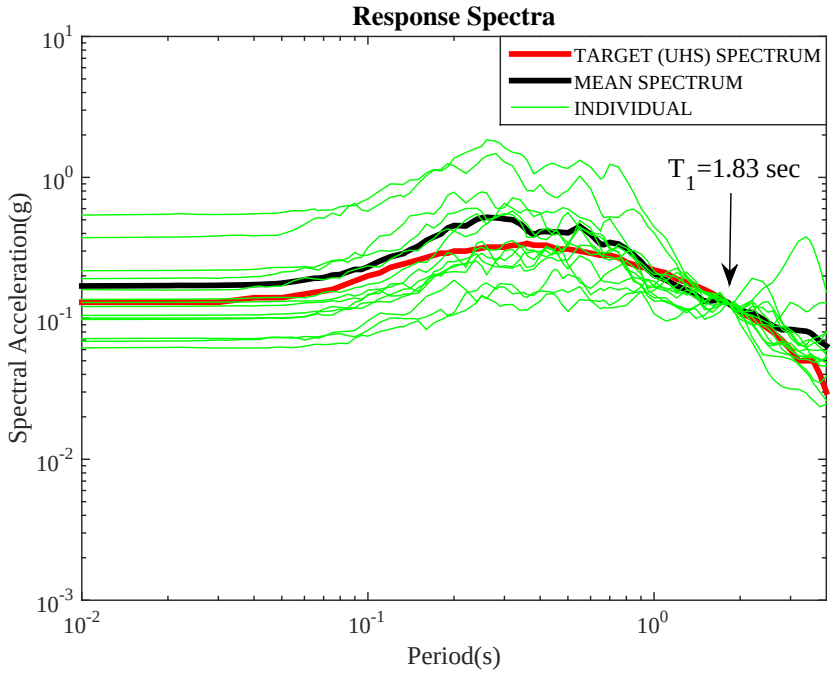


Figure 7.2. Response Spectra of Scaled Ground Motions.

Furthermore, properties of selected records were given in Table 7.1.

Table 7.2. Metadata of Selected Records.

| **Event** | **Magnitude** | **Mechanism** | **Rjb(km)** |
|---|---|---|---|
| Landers | 7.28 | Strike Slip | 89 |
| Landers | 7.28 | Strike Slip | 102 |
| Landers | 7.28 | Strike Slip | 100 |
| Landers | 7.28 | Strike Slip | 107 |
| Hector Mine | 7.13 | Strike Slip | 84 |
| Hector Mine | 7.13 | Strike Slip | 97 |
| El Mayor,Cucapah,Mexico | 7.2 | Strike Slip | 71 |
| El Mayor,Cucapah,Mexico | 7.2 | Strike Slip | 77 |
| El Mayor,Cucapah,Mexico | 7.2 | Strike Slip | 99 |
| El Mayor,Cucapah,Mexico | 7.2 | Strike Slip | 92 |
| El Mayor,Cucapah,Mexico | 7.2 | Strike Slip | 117 |
| El Mayor,Cucapah,Mexico | 7.2 | Strike Slip | 81 |

Overturning moment values at base of chimney obtained under selected earthquake records based on linear time history analysis were obtained. Lognormal distribution was set to analysis results and probability density function was developed for non-updated and updated model as shown in Figure 7.3.

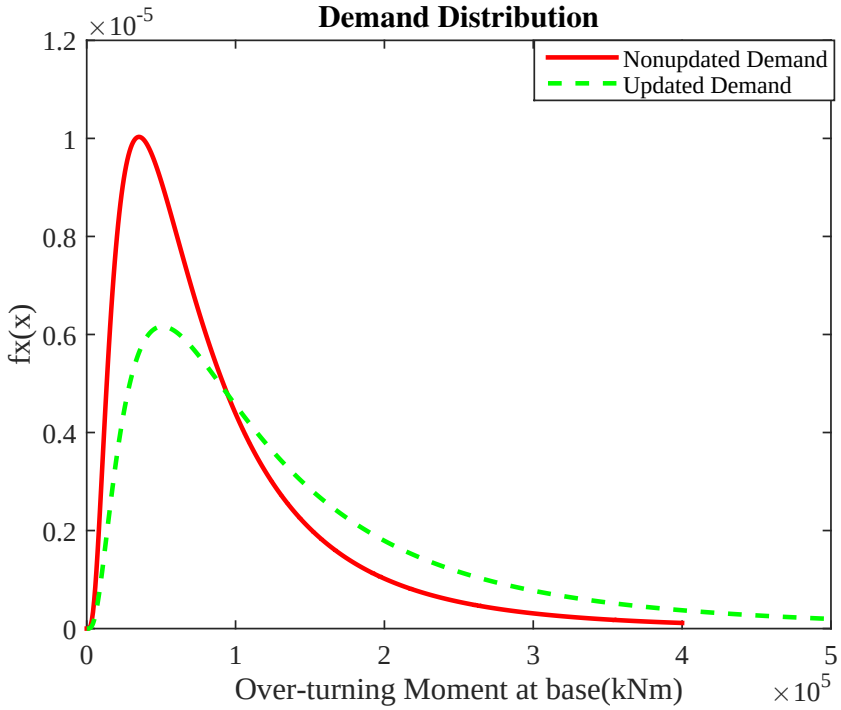


Figure 7.3. Demand Distribution of Structure.

Mean value of demand distribution for non-updated and updated model was found 87025 and 142854 kNm, respectively. C.O.V values were calculated 0.699 and 0.716, respectively.

### 7.1.2. Development of Capacity Distribution

Monte Carlo simulation was used to estimate the mean and C.O.V of ultimate moment capacity of the chimney section at base. Random variables were digitally simulated with specified probability distribution function which has mean and C.O.V values shown as Table 7.2 (Ellingwood, 1980, Mirza *et al.*, 1979, Mirza and Mac Gregor, 1979).

Table 7.3. Statistics of Basic Variables.

| Basic Variables | Mean | COV | PDF |
|---|---|---|---|
| Es | 201188 MPa | 0.033 | Normal |
| fck (C30) | 27.75 MPa | 0.15 | Normal |
| fyk (S420) | 489 MPa | 0.093 | Lognormal |
| ec | 0.003 | 0.16 | Normal |

Expressed in ACI 307-08 were used to obtain moment capacity. The number of simulation cycles was selected as 30000 and capacity distribution was developed presented in Figure 7.4.

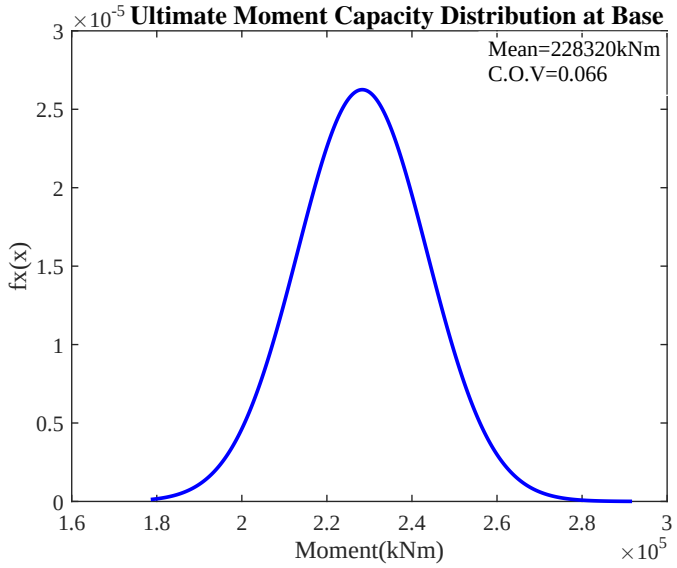


Figure 7.4. Capacity Distribution.

Limit state condition was considered as yield moment capacity in accordance with CICIND (2001). Mean value of ultimate moment capacity was found 228320 kNm and COV value was calculated as 0.066.

### 7.1.3. Reliability Estimation

On the basis of the theoretical principles of reliability analysis, failure probability of system is the cumulative probability where demand is greater than capacity. For this reason, first, the area of this condition was obtained for updated and non-updated cases as seen in Figure 7.5. Afterwards, the structural reliability was found as $1 - P_f$.

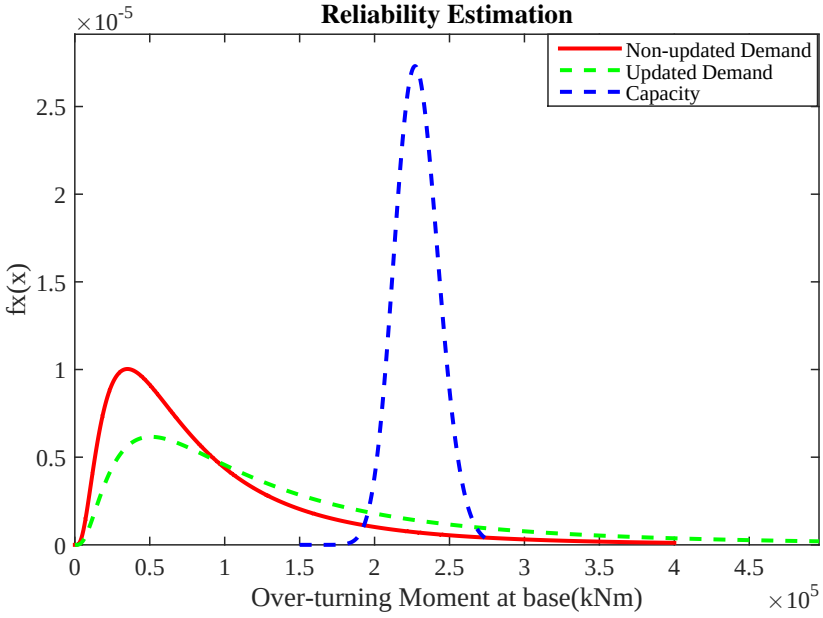


Figure 7.5. Probability Distributions of Capacity and Demand Curves.

Table 7.4. Estimated Probability of Failure Values of the Chimney.

| **Updated** | **Non-updated** |
|---|---|
| $85.10^{-4}$ | $12.10^{-4}$ |

Table 7.6 indicates that an estimated reliability value for updated case is lower than non-updated case. The target probability of failure for this type of chimney is suggested as $10^{-4}$ (CICIND, 2001). Even though, the non-updated case shows such in agreement roughly with CICIND value, however the value for updated case is a little bit far away from that point. Damping ratio value is a key point on that conclusion.

## 7.2. Wind Loading

Reliability estimation of the chimney based on wind analysis with updated and non-updated system was performed. Demand distribution of the chimney was developed depending on overturning moment values at base of chimney obtained under many seeds utilizing multivariate stochastic process.

Capacity distribution of the chimney section was also developed depending on ultimate moment capacity of chimney section at base by using Monte Carlo simulation.

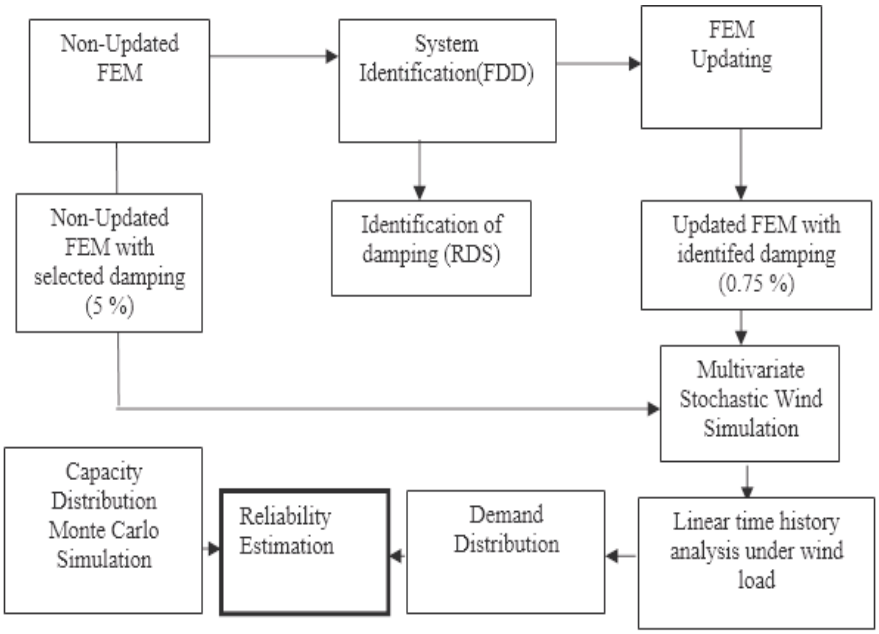


Figure 7.6. The Flowchart that Summarizes All Steps to Estimate Reliability of the Structure.

Reliability of the structure was found by using interference with demand and capacity probability distribution curves. Figure 7.7 shows the flowchart that summarizes all steps to estimate reliability of the structure.

### 7.3. Development of Demand Distribution

Since wind loading has repetitive loading characteristics, enough number of seeds was taken into account. Plotting the ratio mean of maximums based on overturning moment for each seed to maximums versus number of seed might give a rational result. When values on axis y converge to one, the number of seed can be identified. In accordance with this information given, the number of seeds is calculated as 10 (Figure 7.7).

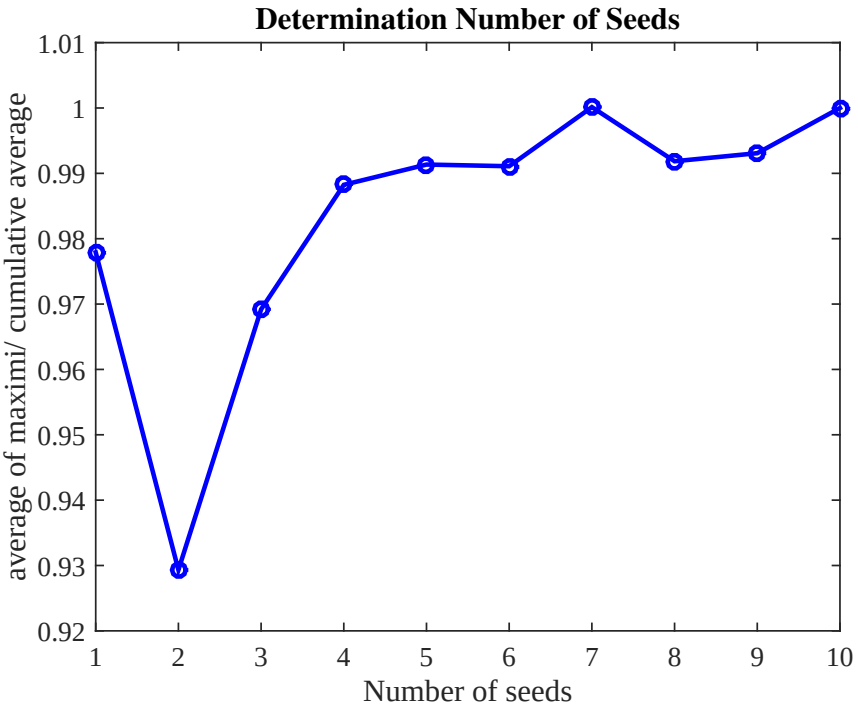


Figure 7.7. Determination of Number of Seeds Running for Mean of Maxima.

Overturning moment values at base of chimney obtained based on linear time history analysis were obtained. Normal (Gaussian) distribution was set to analysis results and probability density function was developed for non-updated and updated model as shown in Figure 7.8.

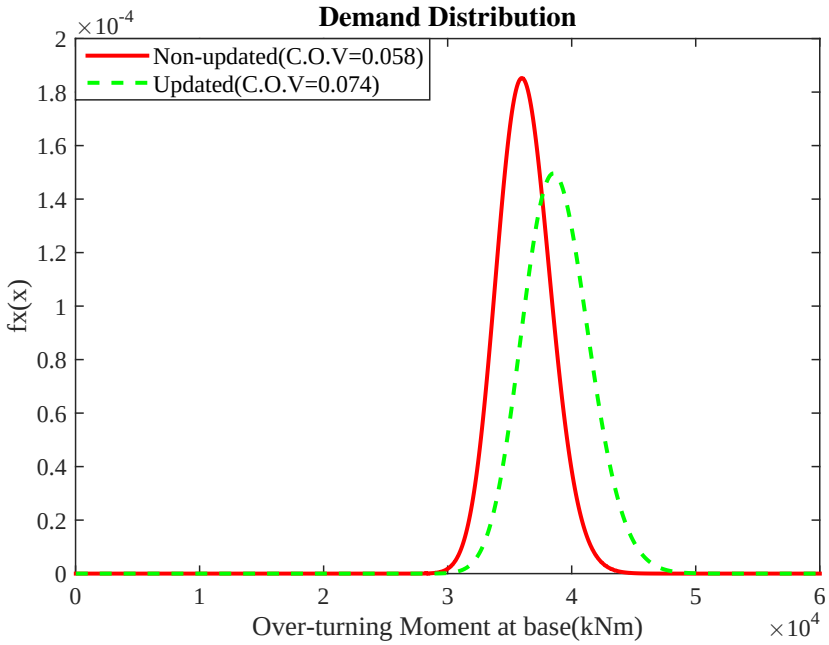


Figure 7.8. Demand Distribution of Structure.

Mean value of demand distribution for non-updated and updated model was found 36171 and 38802 kNm, respectively. C.O.V values were calculated 0.058 and 0.074, respectively.

## 7.4. Developing of Capacity Distribution

A Monte Carlo simulation format was used to estimate the mean and C.O.V of ultimate moment capacity of the chimney section at base. Uncertainties that influence moment capacity of the section were defined as C.O.V ( Ang and Tang, 1975). The random basic variables were digitally simulated with specified probability distribution function which has mean and C.O.V values shown as Table 7.4 (Ellingwood, 1980, Mirza *et al.*, 1979, Mirza and Mac Gregor, 1979).

Table 7.5. Statistics of Basic Variables.

| Basic Variables | Mean | COV | PDF |
|---|---|---|---|
| Es | 201188 MPa | 0.033 | Normal |
| fck (C30) | 27.75 MPa | 0.15 | Normal |
| fyk (S420) | 489 MPa | 0.093 | Lognormal |
| $\varepsilon$c | 0.003 | 0.16 | Normal |

Closed form equations expressed in CICIND-2001 were used to obtain crack moment capacity. The number of simulation cycles was selected as 30000 and capacity distribution was developed presented in Figure 7.9.

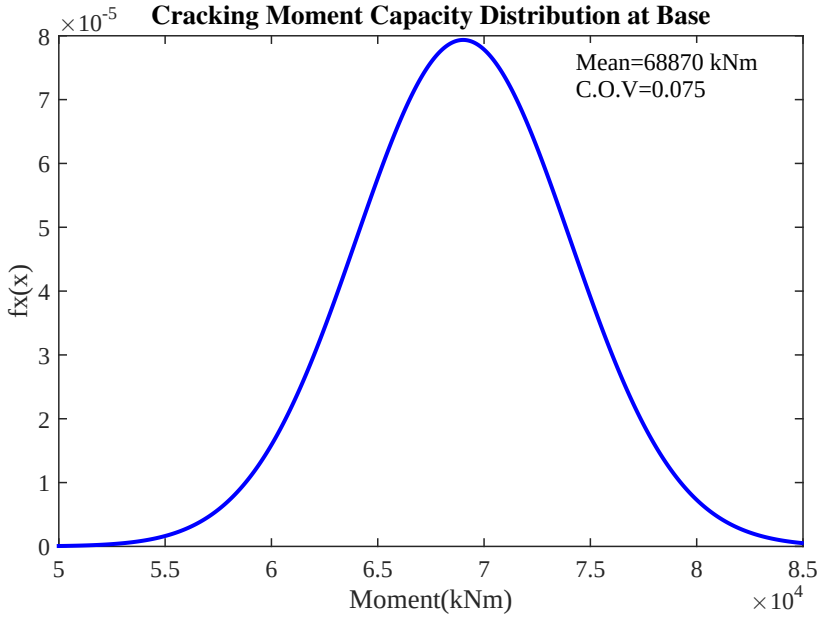


Figure 7.9. Capacity Distribution.

Cracking moment capacity was obtained for serviceability limit state condition under wind loading (CICIND,2001). Mean value of cracking ultimate moment capacity was found 68870 kNm and COV value was calculated as 0.075.

## 7.5. Reliability Estimation

On the basis of the theoretical principles of reliability analysis, failure probability of system is the cumulative probability that demand is greater than capacity. For this reason, first, the area of this condition was obtained for updated and non-updated cases as seen in Figure 7.10. Afterwards, the structural reliability was found as $1 - P_f$.

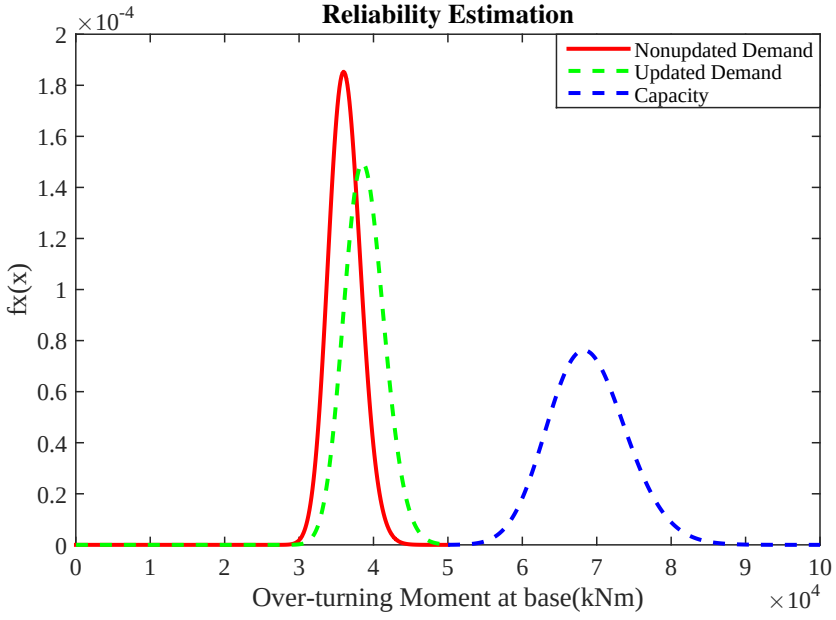


Figure 7.10. Probability Distributions of Capacity and Demand Curves.

Table 7.6. Estimated Probability of Failure Values of the Chimney.

| **Updated** | **Non-updated** |
|---|---|
| 200.10−8 | 3.10−8 |

Table 7.2 indicates that an estimated reliability value for updated case is lower than non-updated case. The target probability of failure for this type of chimney is suggested as 10−8. (CICIND, 2001). The estimated values are in good agreement with the value in CICIND provision.

# 8. CONCLUSION AND FUTURE WORK

## 8.1. Conclusions

This study presents the reliability assessment of a 100.5 m tall reinforced concrete chimney at a glass factory under earthquake and wind loading by using structural health monitoring (SHM) tools. In this study, modal parameter such mode shapes, frequencies and damping were identified by using vibration measurements. Afterwards, FEM of the chimney was updated based on identified parameters.

Demand distribution of the chimney was developed in terms of overturning moment values at base of chimney obtained under many seeds utilizing multivariate stochastic process for wind loading. Demand distribution based on updated and non-updated parameters was obtained by using results from multivariate stochastic process Furthermore; demand distribution based on updated and non-updated parameters was also obtained by using results from PSHA for earthquake loading. Afterwards, capacity distribution was developed with Monte Carlo simulation.

Yield moment capacity distribution was obtained for earthquake loading and cracking moment capacity distribution was developed for wind loading. Eventually, structural reliability of the chimney was estimated by means of demand and capacity distributions. Following conclusions were drawn:

- Modal frequencies and shapes values for non-updated case are so close those obtained from system identification. MAC values of the first and second modes are good correlation between the values obtained from system identification .This indicates that construction details of the chimney is well represented by modeling assumptions used in (FEM).
- Damping ratio estimation is in well agreement with proposed values in the literature. The damping ratio of updated FEM has been assigned as 0.75% for reliability assessment for the further part of this study.

- In the context of this study, structural reliability of the chimney for each loading type estimated based on updated parameters are lower than the one based on non-updated parameters due to fact that the level of damping values were different after the updating procedure.
- As a result of seismic hazard calculations, the trend of the deaggregation results with spectral periods indicates that the probability exceedance of long-period spectral accelerations is controlled by earthquakes that are larger in size and farther from the site than those governing short-period spectral acceleration values. This influences demand distribution of the chimney spectral acceleration values close to the first structural period are higher for larger magnitude earthquakes occurring at far distances.
- Damping ratio estimation is in well agreement with proposed values in the literature. However, damping ratio is proposed 5% in many specifications such as Turkish Seismic Code (TSC) for design purposes. Reliability estimation result shows that the value of damping ratio is so sensitive particularly for the stack like structures.
- The target probability of failure for this type of chimney is suggested as 10-4. (CICIND, 2001).If estimated failure probabilities are beyond this limit, the design should be reviewed again.

## 8.2. Conclusions

- Earthquake and wind loading has significant effects on the chimney structure separately. Further study is needed to obtain reliability estimation of the chimney considering both two effects on the chimney at the same time.
- Acrosswind actions are not primary concern for this chimney; however the influence of acrosswind response on the probability failure of the chimneys can be examined for the critical ones.
- The threshold value used in the linear time history analysis is selected as yield moment. If demand value exceeds beyond this threshold limit, it is assumed that the failure at the base section of chimney will occur. Nonlinear analysis can be carried out in order to identify possible damages which can be occurred during

pre and post earthquake events.

- Linear time history analysis were carried out along one direction. Bidirectional effects can be taken into consideration in the future studies.

# APPENDIX A: DESIGN STRENGTH OF CIRCULAR SHELLS

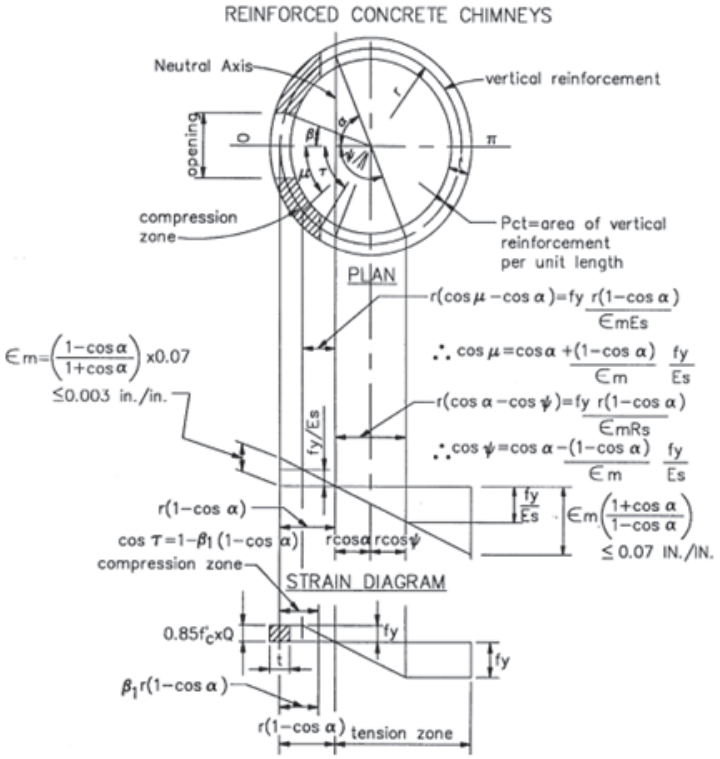


Figure A.1. Stress Diagram.

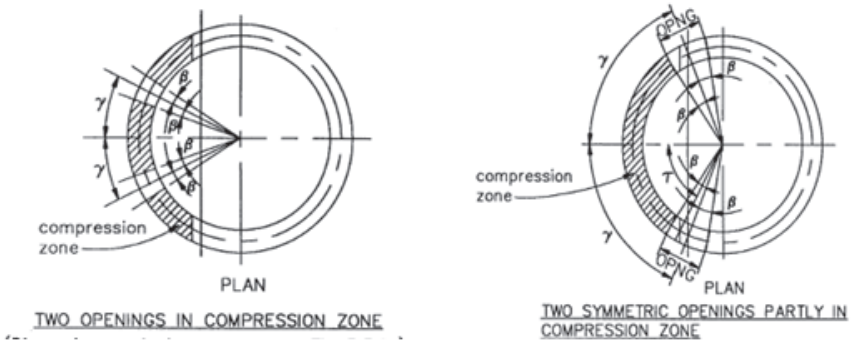


Figure A.2. Two Openings in Compression Zone.

$$P_u/rtf'_c = K_1 = 1.7Q\lambda + 2\varepsilon_m K_e \omega_t Q_1 + 2\omega_t \lambda_1 \tag{A.1}$$

where is the $P_u$ factored vertical load, is the $r$ average radius of section, is the $t$ thickness of section.

$$\lambda = \tau - n\beta(radians) \tag{A.2}$$

$$Q_1 = \frac{sin\psi - sin\mu - (\psi - \mu)cos\alpha}{1 - cos\alpha} \tag{A.3}$$

$$\lambda_1 = \mu + \psi - \pi(radians) \tag{A.4}$$

$\mu, \tau, \psi$= angles shown in

$$cos\tau\beta_1(1 - cos\alpha) \tag{A.5}$$

$$cos\psi = cos\alpha - (\frac{1 - cos\alpha}{\varepsilon_m})(\frac{f_y}{E_s}) \geq -1.0 \tag{A.6}$$

$$cos\mu = cos\alpha - (\frac{1 - cos\alpha}{\varepsilon_m})(\frac{f_y}{E_s}) \leq 1.0 \tag{A.7}$$

where is the $\alpha$ one-half the central angle subtended, is the by neutral axis, is the $\beta$= one-half opening angle, is the $\beta_1$ 0.85 for $f'_c \leq 4000$ psi (27.6 MPa), is the 0.85 - 0.05($f'_c$ - 4000)/1000 $\geq$ 0.65, is the $f'_c > 4000$ psi for metric units, is the $\beta_1$ 0.85 - 0.05($f'_c$ - 27.6)/6.9 $\geq$ 0.65, is the $f'_c > 27.6$ MPa, is the $K_e$ $E_s/f_y$, is the $\omega_t$ $\rho_t f_y/f'_c$, is the $\rho_t$ ratio of total vertical reinforcement to total area of concrete, is the $n_1$ number of openings entirely in compression zone (maximum 2)

$$\varepsilon_m = 0.07(1 - cos\alpha)/(1 + cos\alpha) \leq 0.003 \tag{A.8}$$

$$M_n/P_u r = K_3 = cos\alpha + K_2/K_1, M_n = P_u r K_3 \tag{A.9}$$

$$K_2 = 1.7QR + \varepsilon_m K_e \omega_t Q_2 + 2\omega_t K \tag{A.10}$$

For $\alpha \leq 5$ deg

$$Q = (-0.523 + 0.181\alpha - 0.0154\alpha^2) + (41.3 - 13.2\alpha + 1.32\alpha^2(t/r) \tag{A.11}$$

For 5 deg $< \alpha \leq 10$ deg

$$Q = (-0.1540.01773\alpha + 0.00249\alpha^2) + (16.42 - 1.980\alpha + 0.0674\alpha^2)(t/r) \tag{A.12}$$

For 10 deg $< \alpha \leq 17$ deg

$$Q = (-0.488 + 0.076\alpha) + (9.758 - 0.640\alpha)(t/r) \tag{A.13}$$

For 17 deg $< \alpha \leq 25$ deg

$$Q = (-1.345 + 0.2018\alpha - 0.004434\alpha^2) + (15.83 - 1.676\alpha + 0.03994\alpha^2)(t/r) \tag{A.14}$$

For 25 deg $< \alpha \leq 35$ deg

$$Q = (0.993 - 0.00258\alpha) + (-3.27 + 0.0862\alpha)(t/r) \tag{A.15}$$

For $\alpha > 35$ deg

$$Q = 0.89 \tag{A.16}$$

where $M_n$ nominal moment strength of section

$$Q_2 = \frac{(\psi-\mu)(1+2cos^2\alpha)+(1/2)|(4sin2\alpha+sin2\psi-sin2\mu)-4cos\alpha(sin\alpha+sin\psi-sin\mu)}{(1-cos\alpha)} \tag{A.17}$$

$$K = sin\psi + sin\mu + (\pi - \psi - \mu)cos\alpha \tag{A.18}$$

$$R = sin\tau - (\tau - n_1\beta)cos\alpha - (n_1/2)[sin(\gamma + \beta) - sin(\gamma - \beta)] \tag{A.19}$$

where is the $\gamma$ 1/2 angle between center lines of two openings and for no openings, $n_1 = \gamma = \beta = 0$; for one opening in compression zone, $n_1 = 1, \gamma = 0$; for two openings in compression zone, $n_1 = 2$

Two symmetric openings partly in compression zone Refer. This condition exists when $\gamma + \beta > \tau$ and $\gamma - \beta < \tau$. For this case, let $\delta = \gamma - \beta$.

$$R = sin\delta - \delta cos\alpha \tag{A.20}$$

# REFERENCES


1. ACI 307-08, "Code Requirements for Reinforced Concrete Chimneys and Commentary", American Concrete Institute, USA, 2008.

2. ACI Committee 318, "Building Code Requirements for Structural Concrete (ACI 318-08) and Commentary", *American Concrete Institute*, Farmington Hills, MI, 2008.

3. Akkar S., M.A. Sandikkaya, J.J. Bommer, "Empirical Ground-Motion Models for Point and Extended-Source Crustal Earthquake Scenarios in Europe and the Middle East", *Bull Earthquake Engineering*, Vol. 12, No.1, pp. 359-387, 2014.

4. Ang, A.H., W.H. Tang, "Probability Concepts in Engineering, Emphasis on Applications to Civil & Environmental Engineering", 1st Ed., *John Wiley & Sons*, New Jersey, 1975.

5. Baker, J.W., C.A. Cornell, "Spectral Shape, Epsilon and Record Selection", *Earthquake Engineering & Structural Dynamics*, Vol. 35, No 9, pp. 1077-1095, 2006.

6. Bazzurro P., C.A. Cornell, "Disaggregation of Seismic Hazard", *Bulletin of the Seismological Society of America*, Vol. 89, No. 2, pp. 501-520, 1999.

7. Brownjohn J.M.W., E.P. Carden, C.R. Goddard, G. Oudin, "Real-Time Performance Monitoring of Tuned Mass Damper System for a 183 m Reinforced Concrete Chimney", *Journal of Wind Engineering and Industrial Aerodynamics*, Vol. 98, No. 3, pp. 169-179, 2010.

8. BS EN 1992-1-1, "Eurocode 2: Design of Concrete Structures", *British Standard Institution*, London, 2005.

9. Burrough, H.L., A.P. Jeary, J.M. Wilson, "Vibration Measurements on the Drax

Gas Turbine Chimney, Central Electricity Research Labs", RD/L/N 167/72, *Leatherhead*, Surrey, 1972.

10. Cheng, C.M., A. Kareem, "Acrosswind Response of Reinforced Concrete Chimneys", *Journal of Wind Engineering and Industrial Aerodynamics*, Vol. 41-44, pp. 2141-2152, 1992.

11. Chopra A.K., "Dynamics of Structures, Theory and Application to Earthquake Engineering" 3rd Ed., *Pearson-Prentice Hall*, New Jersey, 2011.

12. "CICIND Model Code for Concrete Chimneys and Commentary", 2nd Ed, *Ratingen*, Germany, 2001.

13. Cole A., "On-Line Failure Detection and Damping Measurement of Aerospace Structures by Random Decrement Signature", *NASA CR 2205*, 1979.

14. Cornell, C.A., "Engineering Seismic Risk Analysis", *Bulletin of the Seismological Society of America*, Vol. 58, pp. 1583-1606, 1968.

15. Davenport, A.G., "The Dependence of wind Load Upon Meteorological Parameters. InProcude of the International Resistance Seminar of Wind Effects on Building and Struct., Vol. 1, pp. 19-82, 1968.

16. Deodatis, G. and M. Shinozuka, "Simulation of Seismic Ground Motion Using Stochastic Waves", ASCE, *Journal of Engineering Mechanics*, Vol. 115, No. 12, pp. 2723-2737, 1989.

17. Deodatis, G., "Simulation of Ergodic Multivariate Stochastic Processes", *Journal of Engineering Mechanics*, Vol. 122, No. 8, pp. 778-787, 1996.

18. Doebling S.W, C.R. Farrar, M.B. Prime, D.W. Shevitz, "Damage Identification and Health Monitoring of Structural and Mechanical Systems from Changes in their Vibration Characteristics: A Literature Review", *Los Alamos National Laboratory Report*, LA-13070-MS, 1996.

19. Dowrick D.J., D.A. Rhoades, "Relations Between Earthquake Magnitude and Fault Rupture Dimensions: How Regionally Variable Are They", *Bulletin of the Seismological Society of America*, Vol. 94, No. 3, pp. 776-788, 2004.

20. Ellingwood, B., T.V. Galambos, J.G. MacGregor, C.A. Cornell, "Development of a Probability Based Load Criterion for American National Standard A58." Special Publication No. 577, *National Bureau of Standards*, 1980.

21. Ellingwood, B., T.V. Galambos, J.G. MacGregor, C.A. Cornell, "Development of a Probability Based Load Criterion for American National Standard, , A58", Special Publication No. 577, National Bureau of Standards, 1980.

22. Field E.H., T.H. Jordan, C.A. Cornell, "Open SHA: A Developing Community-Modeling Environment for Seismic Hazard Analysis", *Seismological Research Letters* Vol. 74, No. 4, 2003.

23. Field E., V. Gupta, N. Gupta, P. Maechling, T. Jordan, "Hazard Calculations for the WGCEP-2002 Earthquake Forecast Using Open SHA and Distributed Object Technologies", *Seismological Research Letters*, Vol. 76, No. 2, 2005.

24. Field E., V. Gupta, N. Gupta, P. Maechling, T. Jordan, "Hazard Map Calculations Using Grid Computing", *Seismological Research Letters*, Vol. 76, No. 5, 2005.

25. Ghanem, R., M. Shinozuka, "Structural System Identification I: theory", *Journal of Engineering Mechanics*, Vol. 121, No. 2, pp. 255-264, 1995.

26. Gözrski P., "Investigation of Dynamic Characteristics of Tall Industrial Chimney Based on GPS Measurements Using Random Decrement Method", *Engineering Structures*, Vol. 83, pp. 30-49, 2015.

27. Goyal A., M.K. Maiti, "Inelastic Seismic Resistance of Reinforced Concrete Stack-like Structure", *Earthquake Engineering and Structural Dynamics*, Vol. 26, pp. 501-513, 1997.

28. Gulkan P, "Expecting the Expected: 1g Peak Motions in the Istanbul Metropolitan Area", *15 th World Conference on Earthquake Engineering*, 2012.

29. Halabian A.M., S. Kabiri, "Effect of Foundation Flexibility on Ductility Reduction Factors for R/C Stack-Like Structures", *Earthquake Engineering and Engineering Vibration*, Vol. 10, No. 2, pp. 277-290, 2011.

30. Holmes. J.D., "Wind loading of Structures", *Spon Press*, London, 2001.

31. Kaimal J.C., J.C. Wyngaard, Y. Izumi, O.R. Cot, "Spectral Characteristics of Surface-Layer Turbulence", *Journal Royal Meteorological Society*, Vol. 98, pp. 563-589, 1958.

32. Kalkan E., P. Gulkan, "Site-Dependent Spectra Derived from Ground Motion Records in Turkey",*Earthquake Spectra*, Vol. 20, No. 4, pp. 1111-1138, 2004.

33. Kareem A., J. Hsieh, "Reliability Analysis of Concrete Chimneys Under Wind Loading', *Journal of Wind Engineering and Industrial Aerodynamics*, Vol. 25, No. 1, pp. 93-112, 1986.

34. Kareem A, J. Hsieh, "Statistical Analysis of Tubular R/C Sections", *Journal of Structural Engineering*, ASCE, Vol. 114, No. 1, pp. 900-916, 1988.

35. Kareem A, J. Hsieh, "Reliability Analysis of Concrete Chimneys Under Wind Loading", *Journal of Wind Engineering and Industrial Aerodynamics*, Vol. 25, No. 1, pp. 93-112, 1986.

36. Li, Y., A. Kareem, "Simulation of Multi-Variate Nonstationary Random Processes by FFT", *Journal of Engineering Mechanics*, ASCE, Vol.117, No.5, pp. 1037-1058, 1991.

37. MacGregor, J.G., S.A. Mirza, B. Ellingwood, "Statistical Analysis of Resistance of Reinforced and Prestressed Concrete Members", Am. Concr. Inst., Vol. 80, No. 3, pp. 167-176, 1983.

38. Maia, N.M.M., J.M.M. Silva, "Modal Analysis Identification Ttechniques", *Philosophical Transactions of the Royal Society*, Vol. 359, pp. 29-40, 2001.

39. Menon, D., P.R. Rao, "Uncertainties in Codal Recommendations for Across-wind Load Analysis of R/C Chimneys", *Journal of Wind Engineering and Industrial Aerodynamics*, Vol. 72, pp. 455-468, 1997.

40. Moaveni B, J.P. Conte, F.M. Hemez, "Uncertainity and Sensitivity Analysis of Damage Identification Results Obtained Using Finite Element Model Updating", C*omputer-Aided Civil and Infrastructure Engineering*, Vol. 24, pp. 320-334, 2009.

41. Otte, D., P.V.D. Ponseele, J. Leuridan, "Operational Shapes Estimation as a Function of Dynamic Loads, in Proceedings of 8th International Modal Analysis Conference", *Society for Experimental Mechanics*, Vol. 1, pp. 413-21, 1990.

42. Scruton, C., D.A. Harding, "Measurement of the Structural Damping of a Reinforced Concrete Chimney Stack at Ferrybridge 'B' Power Station", *NPL Aero Report* NPL/Aero/323, 1957.

43. Shinozuka M, "Seismic Reliability of Concrete Beams", *Journal of Structural Engineering*, ASCE, Vol. 109, No. 7, pp. 1617-1634, 1983.

44. Shinozuka M, C.M. Jan, "Digital Simulation of Random Processes and its Applications", *Journal of Sound and Vibration*, Vol. 25, No. 1, pp. 111-128. 1972.

45. Shinozuka, M., M. Kamata, C.B. Yun, "Simulation of Earthquake Ground Motion as Multi-Variate Stochastic Process", *Princeton-Kajima Joint Resistance*, Princeton, N.J, 1989.

46. Shinozuka, M., S.T. Ariaratnam, H.E.H. Leipholz, "Digital Simulation of Random Processes in Engineering Mechanics with the Aid of the FFT Technique", *In Stochastic Problems in Mechanics*, Vol. 1, pp. 277-286, 1974.

47. Simiu E., R.H. Scanlan "Wind Effects on Structures", John Wiley & Sons, 1986.

48. Skolnik D., Y, Lei, E. Yu and J. Wallace, "Identification, Model Updating and Response Prediction of an Instrumented 15-Story Steel-Frame Building", *Earthquake Spectra*, Vol. 22, No. 3, pp. 781-802, 2006.

49. Sohn, H., C.R. Farrar, F.M. Hemez, D.D. Shunk, D.W. Stinemates, B.R. Nadler, J.J. Czarnecki, "A Review of Structural Health Monitoring Literature", *Los Alamos National Laboratory Report*, LA-13976-MS, 2004.

50. Vickery B.J., R. Basu, "Across-wind Vibrations of Structures of Circular Cross Section. Part 1. Development of a Mathematical Model For Two Dimensional Conditions", *Journal of Wind Engineering and Industrial Aerodynamics*, Vol. 12, pp. 75-97, 1998.

51. Vickery B.J., R. Basu, "Across-wind Vibrations of Structures of Circular Cross Section.Part 2. Development of a Mathematical Model For Two Dimensional Conditions", *Journal of Wind Engineering and Industrial Aerodynamics*, Vol. 12, pp. 98-118, 2005.

52. Vickery B.J., R. Basu, "The Response of Reinforced Concrete Chimneys to Vortex Shedding", *Engineering Structures*, vol. 6, pp. 324-333, 1984.

53. Vickery B.J, R. Basu "Simplified Approaches to the Evaluation of the Across-wind Response of Chimneys", *Journal of Wind Engineering and Industrial Aerodynamics*, Vol. 1, pp, 153-166, 1983.

54. Wilson J.L, "Earthquake Response of tall Reinforced Concrete Chimneys", *Engineering Structures*, Vol. 25, pp. 11-24, 2002.

55. Wilson J.L, "The Cyclic Behavior of Reinforced Concrete Chimney Section With and Without Openings", *CICIND Report* CR 19-2.